PNAS RESEARCH ARTICLE | NEUROSCIENCE

Neuronal activity-induced, equilibrative nucleoside transporter-dependent, somatodendritic adenosine release revealed by a GRAB sensor

Zhaofa Wu[a,b,c,1], Yuting Cui[d,e,1], Huan Wang[a,b,1], Hao Wu[f], Yi Wan[a,b,c], Bohan Li[a,b,c], Lei Wang[a,b,g], Sunlei Pan[a,b,c], Wanling Peng[h], Ao Dong[a,b,c], Zhengwei Yuan[d,f], Miao Jing[e], Min Xu[h], Minmin Luo[d,e,i,j,k,2], and Yulong Li[a,b,c,l,m,n,2]

Edited by Richard Tsien, New York University Grossman School of Medicine, New York, NY; received July 19, 2022; accepted February 28, 2023

The purinergic signaling molecule adenosine (Ado) modulates many physiological and pathological functions in the brain. However, the exact source of extracellular Ado remains controversial. Here, utilizing a newly optimized genetically encoded GPCR-Activation-Based Ado fluorescent sensor ($GRAB_{Ado}$), we discovered that the neuronal activity–induced extracellular Ado elevation is due to direct Ado release from somatodendritic compartments of neurons, rather than from the axonal terminals, in the hippocampus. Pharmacological and genetic manipulations reveal that the Ado release depends on equilibrative nucleoside transporters but not the conventional vesicular release mechanisms. Compared with the fast-vesicular glutamate release, the Ado release is slow (~40 s) and requires calcium influx through L-type calcium channels. Thus, this study reveals an activity-dependent second-to-minute local Ado release from the somatodendritic compartments of neurons, potentially serving modulatory functions as a retrograde signal.

adenosine | neuronal activity | somatodendrite | ENT transporter

Significance

Adenosine (Ado) is a critical neuromodulator, which has been implicated in many physiological and pathological processes such as sleep–wake regulation, learning and memory, epilepsy, and stroke. However, a fundamental question regarding the exact mechanism of Ado release in the brain is still far from clear, partly due to the lack of a sensitive method for its chemical- and cell-type-specific detection with high spatiotemporal resolution. Using a newly optimized genetically encoded fluorescent Ado sensor ($GRAB_{Ado}$); in combination with glutamate imaging, pharmacology, and genetic manipulation, we reveal the somatodendritic release of endogenous Ado with molecular details.

Extracellular adenosine (Ado) participates in many physiological processes, including the sleep–wake cycle, learning and memory, cardiovascular function, and immune responses (1–4). Impaired adenosinergic signaling has been implicated in various diseases and pathological conditions such as pain, migraine, epilepsy, stroke, drug addiction, and neurodegeneration (e.g., Parkinson's disease) (2, 5, 6). In the brain, Ado acts as a neuromodulator or a homeostatic modulator at the synaptic level by activating corresponding G protein-coupled receptors (GPCRs) (7). Although Ado's function has been extensively studied, a fundamental question regarding the source of extracellular Ado in the brain is still under debate.

At the cellular level, Ado can be released from neurons (8) and/or adjacent, nonneuronal cells, such as astrocytes (9). At the subcellular level, it has been suggested by ^3H labeling of Ado derivatives that Ado could be released from central axon terminals (10). In contrast, direct intracellular loading of Ado in a single pyramidal neuron in the hippocampal CA1 region can inhibit excitatory postsynaptic potentials via presynaptic A1 receptors (11), which suggests that neuronal somatodendritic compartments are capable of releasing Ado to modulate synaptic functions retrogradely. However, whether the endogenous Ado can be released from the somatodendritic compartment needs to be better understood. At the molecular level, Ado may be produced by the degradation of extracellular adenosine 5′-triphosphate (ATP) (12) via the CD39-CD73 enzyme cascade (13). Alternatively, Ado may be released directly from neurons via nucleoside transporters (8, 14) or by vesicular exocytosis (15).

The difficulty in studying the source of extracellular Ado and the mechanisms underlying Ado release lies in the complexity of the Ado system and the supreme complexity of the brain network. Moreover, the lack of sensitive methods for directly visualizing Ado release with high spatiotemporal resolution confined the understanding of Ado signaling (16, 17). Recently, we developed a genetically encoded GPCR-Activation-Based (GRAB) adenosine sensor, $GRAB_{Ado1.0}$, which can reliably measure changes in extracellular Ado levels in the basal forebrain of living mice (18). Here, we further improved the Ado sensor and combined this tool with pharmacological and genetic experiments to examine the detailed mechanism underlying a neuronal activity–induced Ado release in the hippocampus.

Results

Imaging Ado Release in Hippocampal Brain Slices with a Newly Optimized GRAB Sensor. The four Ado receptors in mammals show very variable Ado affinity (from nanomolar to micromolar) (19) and thus suggest an extensive range of working concentrations.

Author contributions: Z.W., Y.C., M.X., M.L., and Y.L. designed research; Z.W., Y.C., H. Wang, H. Wu, Y.W., B.L., L.W., S.P., W.P., A.D., Z.Y., and M.J. performed research; Z.W., Y.C., H. Wang, H. Wu, Y.W., B.L., L.W., S.P., W.P., A.D., Z.Y., M.X., M.L., and Y.L. analyzed data; and Z.W., M.L., and Y.L. wrote the paper.

The authors declare no competing interest.

This article is a PNAS Direct Submission.

[1]Z.W., Y.C., and H. Wang contributed equally to this work.

[2]To whom correspondence may be addressed. Email: luominmin@nibs.ac.cn or yulongli@pku.edu.cn.

This article contains supporting information online at https://www.pnas.org/lookup/suppl/doi:10.1073/pnas.2212387120/-/DCSupplemental.

Published March 30, 2023.

Previously developed Ado1.0 sensor showed high affinity to Ado (EC_{50} ~60 nM) and modest fluorescence changes to the saturated concentration of Ado (18). The high affinity of Ado1.0 makes it very sensitive to monitor Ado dynamics during sleep-wake cycles (18). However, the fluorescence signal of Ado1.0 becomes easily saturated when the concentration of Ado is more than 1 μM. In acute brain slices of the medial prefrontal cortex (mPFC), we could not detect a robust fluorescence increase of Ado1.0 (*SI Appendix*, Fig. S1 *A–D*). Interestingly, the application of the $A_{2A}R$ antagonist, ZM-241385, substantially reduced the "baseline" fluorescence signal of Ado1.0 (*SI Appendix*, Fig. S1 *E* and *F*). These data suggested that the basal levels of Ado present in acute brain slices (20) might saturate the high-affinity Ado1.0 sensor. To better monitor Ado dynamics in distinct preparations under physiological and pathophysiological conditions, a sensor with both lower affinity and a larger maximum response to Ado is necessary. To achieve that, we optimized the Ado1.0 sensor and generated a new sensor, Ado1.0m, by introducing an M270H mutation in the $A_{2A}R$ backbone of Ado1.0 (Fig. 1*A*). Ado1.0m showed enhanced dynamic range (averaged max $\Delta F/F_0$, Ado1.0m ~350% versus Ado1.0 ~110%) and decreased apparent affinity (EC_{50}, Ado1.0m ~3.2 μM versus Ado1.0 ~0.03 μM) in response to Ado in cultured neurons (Fig. 1 *A–C*). Ado1.0m could barely respond to ATP, and Ado-induced fluorescence signal was not observed when adding $A_{2A}R$ antagonist ZM-241385, suggesting the specificity of Ado1.0m (Fig. 1 *D–F*). To test whether Ado1.0m could be used to detect the endogenous release of Ado, we expressed Ado1.0m in the mPFC using an adeno-associated virus (AAV). After 2 to 3 wk, we prepared the acute mPFC brain slices and imaged the fluorescence response of Ado1.0m. Applying electrical stimuli at 10 Hz for 1 s elicited a robust and repeatable increase in Ado1.0m fluorescence, which was blocked by applying the $A_{2A}R$ antagonist, ZM-241385 (Fig. 1 *G–J*, and *SI Appendix*, Fig. S1). Moreover, increasing the number of stimuli at 10 Hz caused progressively increased responses in Ado1.0m-expressed, but not Ado1.0mut control-expressed acute mPFC brain slices (*SI Appendix*, Fig. S1 *G–K*). These results indicated that the optimized Ado1.0m sensor enables specific imaging of electrical stimulation-triggered endogenous Ado release in acute mPFC brain slices with high sensitivity.

After validating the sensor in mPFC brain slices, we next imaged Ado release in hippocampus brain slices with well-defined anatomical projections. To monitor Ado release and neuronal activity simultaneously, we expressed Ado1.0m and a membrane-targeted jRGECO1a (mjRGECO1a) in CA3 neurons of wild-type mice, placed an electrical stimulation electrode within the CA1, and then performed imaging within the CA1 region, which receives Schaffer collateral inputs from CA3 neurons (Fig. 1*K*). The expression of Ado1.0m and mjRGECO1a on CA3 axons innervating the CA1 region was confirmed (Fig. 1*L*). Electrical stimuli (30 Hz, 100 pulses) produced a robust Ado1.0m response (Fig. 1 *M–O*). The same number of local electrical stimuli (20 pulses) applied at different frequencies (2, 5, 20, and 50 Hz) produced Ado1.0 signals with similar peak amplitudes (*SI Appendix*, Fig. S2 *A–D*). Coapplication of the AMPA receptor antagonist, NBQX, and the NMDA receptor antagonist, D-AP5, significantly reduced the Ado signals but not Ca^{2+} signals in axonal terminals (Fig. 1 *M–O*). NBQX alone or D-AP5 alone did not significantly affect the CA3 axonal Ca^{2+} signals or the Ado1.0m signals (*SI Appendix*, Fig. S3). These results suggested that presynaptic depolarization may contribute to the Ado release in hippocampal CA1 regions.

$GRAB_{Ado}$ Reveals Somatodendritic Ado Release in Hippocampal Slices. We then asked about the source of Ado detected at CA1. When we did electrical stimulation in the CA1 region, NBQX and D-AP5 only partially blocked Ado release (Fig. 1 *M–O*); the remaining might be contributed by the activation of CA1 somatodendrites or CA3 axons or both. Since electrical stimulation lacks cell type- and compartment-specificity, we switched to optogenetic methods. Specifically, to examine whether CA1 somatodendrites can release Ado, we coexpressed mCherry- or tdTomato-tagged light-activated ChrimsonR and Ado1.0m in the hippocampal CA1 neurons, which allowed us to use optogenetics to specifically activate CA1 glutamatergic neurons while simultaneously measuring cell-autonomous activation-evoked Ado release (Fig. 2 *A* and *B*). The same time duration of 633-nm laser stimuli (30 s) applied at different frequencies (2, 5, 10, and 20 Hz) produced Ado1.0m signals with a tendency of progressive increase (*SI Appendix*, Fig. S2 *E–H*). Increasing the number of 633-nm laser pulses applied at 20 Hz induced a progressively increased fluorescence response in the somata, apical dendrites, and basal dendrites of CA1 pyramidal neurons (Fig. 2 *C* and *D*), suggesting that the somatodendritic compartments of CA1 glutamatergic neurons can release Ado under physiological relevant stimulation.

To examine the contributions of CA3 axonal terminals on Ado release detected at CA1, we expressed Ado1.0m in the CA1 region and FLEX-ChrimsonR in the CA3 region of CaMKIIα-Cre knock-in mice (Fig. 2 *E* and *F*). We then used a 633-nm laser to activate the axons of CA3 in the CA1 region. As controls, we performed calcium (Ca^{2+}) imaging or electrophysiological recordings at CA1 neurons at CA3 axon terminals, confirming that this approach effectively activated CA3 axon terminals (*SI Appendix*, Fig. S4 *A–G*). When Ado release was detected, increasing the number of 633-nm laser pulses applied at 20 Hz induced an increased fluorescence response of Ado1.0m in CA1 regions (Fig. 2 *G* and *H*). To test whether the Ado release is attributed to CA3 axonal release or the activation of CA1 somadendrites via glutamate signaling, brain slices were treated with the AMPA receptor antagonist NBQX and the NMDA receptor antagonist D-AP5. Coapplication of NBQX and D-AP5 significantly reduced the Ado1.0m signals (Fig. 2 *G* and *H*), suggesting that the Ado release was mainly contributed by the activation of CA1 somadendrites induced by the glutamate signaling.

Furthermore, we expressed Ado1.0m and FLEX-ChrimsonR in the CA3 region of CaMKIIα-Cre knock-in mice, allowing us to optogenetically activate CA3 terminals at the CA1 region and simultaneously monitor Ado release (*SI Appendix*, Fig. S4 *H* and *I*). Consistently, activating the CA3 axonal terminals in the presence of NBQX & D-AP5 did not evoke a detectable increase in Ado1.0m fluorescence at the CA3 axon terminals. In contrast, local electrical stimuli still produced a robust increased Ado1.0m response (*SI Appendix*, Fig. S4 *J* and *K*). Similarly, chemogenetic activation of CA3 glutamatergic neurons did not evoke Ado release from the axons (*SI Appendix*, Fig. S5). Thus, these results suggested that the axon terminals of CA3 glutamatergic neurons do not directly release Ado.

$GRAB_{Ado}$ Reveals Activity-Dependent Ado Release from Hippocampal Cultures. After the identification of compartmental specific release of Ado in acute hippocampal slices, under physiological-relevant stimulation conditions, we next investigate the detailed molecular mechanisms underlying the neuronal activity–induced Ado release (Fig. 3*A*). In cultured hippocampal neurons expressing Ado1.0, either electrical stimuli (30 Hz, 100 pulses) or application of high extracellular K^+ (75 mM) evoked robust and long-lasting fluorescence increases in both the somata and neuronal processes (Fig. 3 *B–D*). The $A_{2A}R$ antagonist ZM-241385 or SCH-58261 blocked the stimuli-evoked increase in

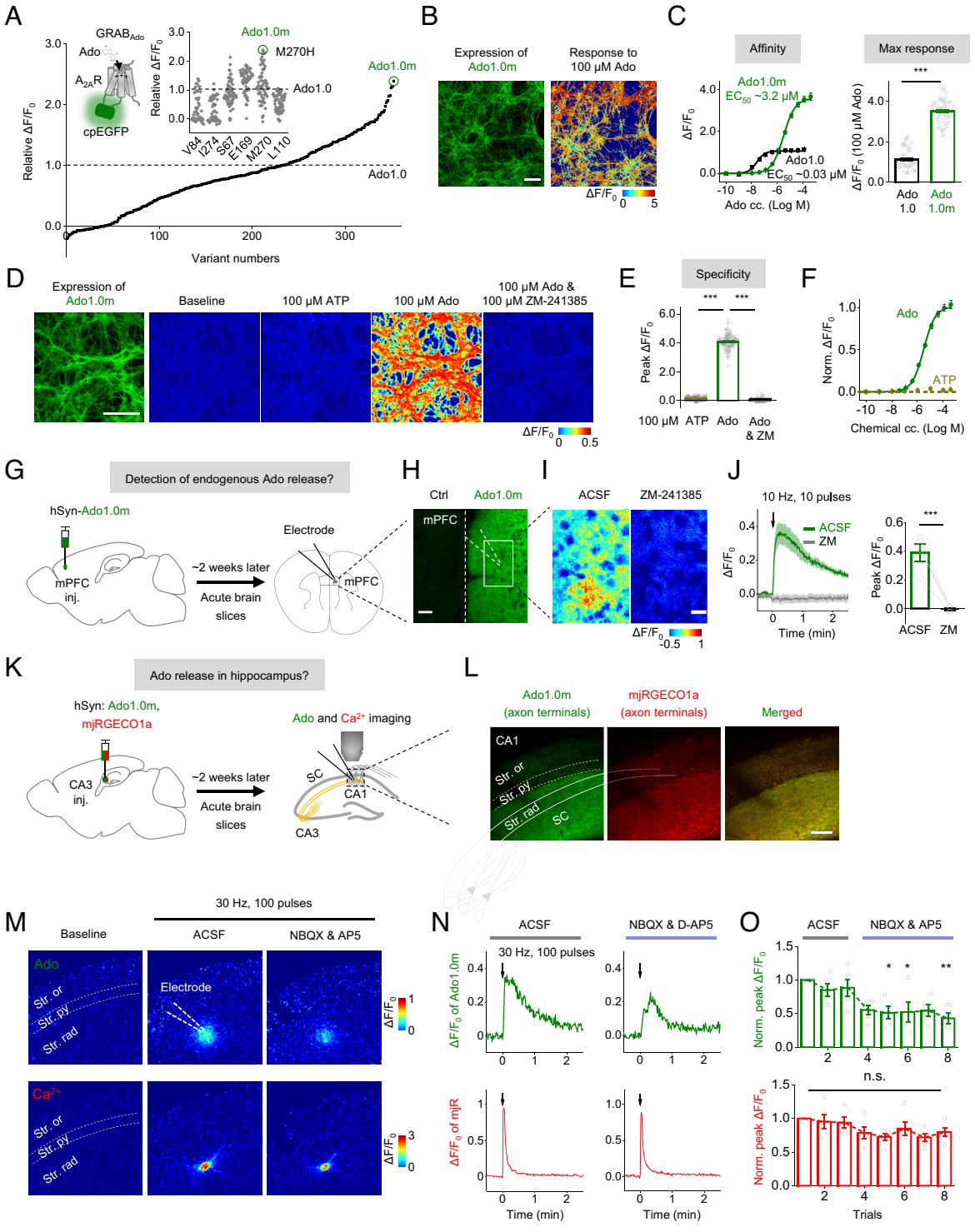

Fig. 1. Detecting adenosine release in the hippocampus with a newly optimized GRAB sensor. (*A*) Generation of a new Ado sensor with medium affinity (Ado1.0m) by introducing mutations on the ligand-binding pockets of human $A_{2A}R$. (*B* and *C*) Fluorescence and pseudocolor images (*B*), dose-response curves (*C*, *Left*), and peak $\Delta F/F_0$ (*C*, *Right*) for Ado1.0 and Ado1.0m sensor in cultured neurons in response to adenosine (Ado); n = 60 ROIs from 3 cultures per group. (*D* and *E*) Expression of Ado1.0m, pseudocolor images (*D*), a summary of Ado1.0m $\Delta F/F_0$ (*E*) in response to ATP, Ado, and ZM-241385 in cultured hippocampal neurons. (*F*) Dose–response curves for Ado1.0m sensor in cultured neurons in response to ATP and Ado. The dose–response curve of Ado is replotted from (*C*). (*G*) Schematic illustration depicting the expression of Ado1.0m or Ado1.0mut in the mouse mPFC, an acute brain slice containing the mPFC, and the placement of a bipolar stimulating electrode in the mPFC. (*H*) Fluorescence images show the expression of Ado1.0m in the ipsilateral mPFC, with no expression in the contralateral mPFC. (*I*) Pseudocolor images of Ado1.0m $\Delta F/F_0$ in response to 10 electrical pulses at 10 Hz delivered in control solution (ACSF) or solution containing the $A_{2A}R$ antagonist ZM-241385 (ZM, 1 μM). (*J*) Traces (*Left*) and group summary (*Right*) of Ado1.0m $\Delta F/F_0$ in response to 10 electrical pulses at 10 Hz delivered ACSF or solution containing the ZM; n = 4 slices from one mouse each. (*K*) Schematic illustration depicting the strategy used to image acute hippocampal brain slices prepared from mice expressing Ado1.0m and membrane-targeted jRGECO1a (mjRGECO1a) in the CA3 region while using an electrode to induce Ado release in the CA1 region. (*L*) Fluorescence images of the CA1 region showing Ado1.0m (green) and mjRGECO1a (red) in CA1 regions. The pyramidal cell layer (Str. py) is located between the stratum oriens (Str. ori) and stratum radiatum (Str. rad). (*M–O*) Pseudocolor images (*M*), traces (*N*), and group summary (*O*) of Ado1.0m $\Delta F/F_0$ in response to 100 pulses applied at 30 Hz in the absence (ACSF) and presence of NBQX & D-AP5; n = 5 slices from 3 mice. (Scale bars represent 100 μm in (*B*, *D*, and *L*), 50 μm in (*H*), and 20 μm in (*I*).) Summary data are presented as the mean ± SEM. Statistical significance in (*C*, *E*, and *J*) was assessed using Student's *t* test; statistical significance in (*O*) was assessed using a one-way ANOVA followed by Bonferroni's multiple comparison test; ***$P < 0.001$; **$P < 0.01$; *$P < 0.05$; n.s., not significant. See also *SI Appendix*, Figs. S1–S3.

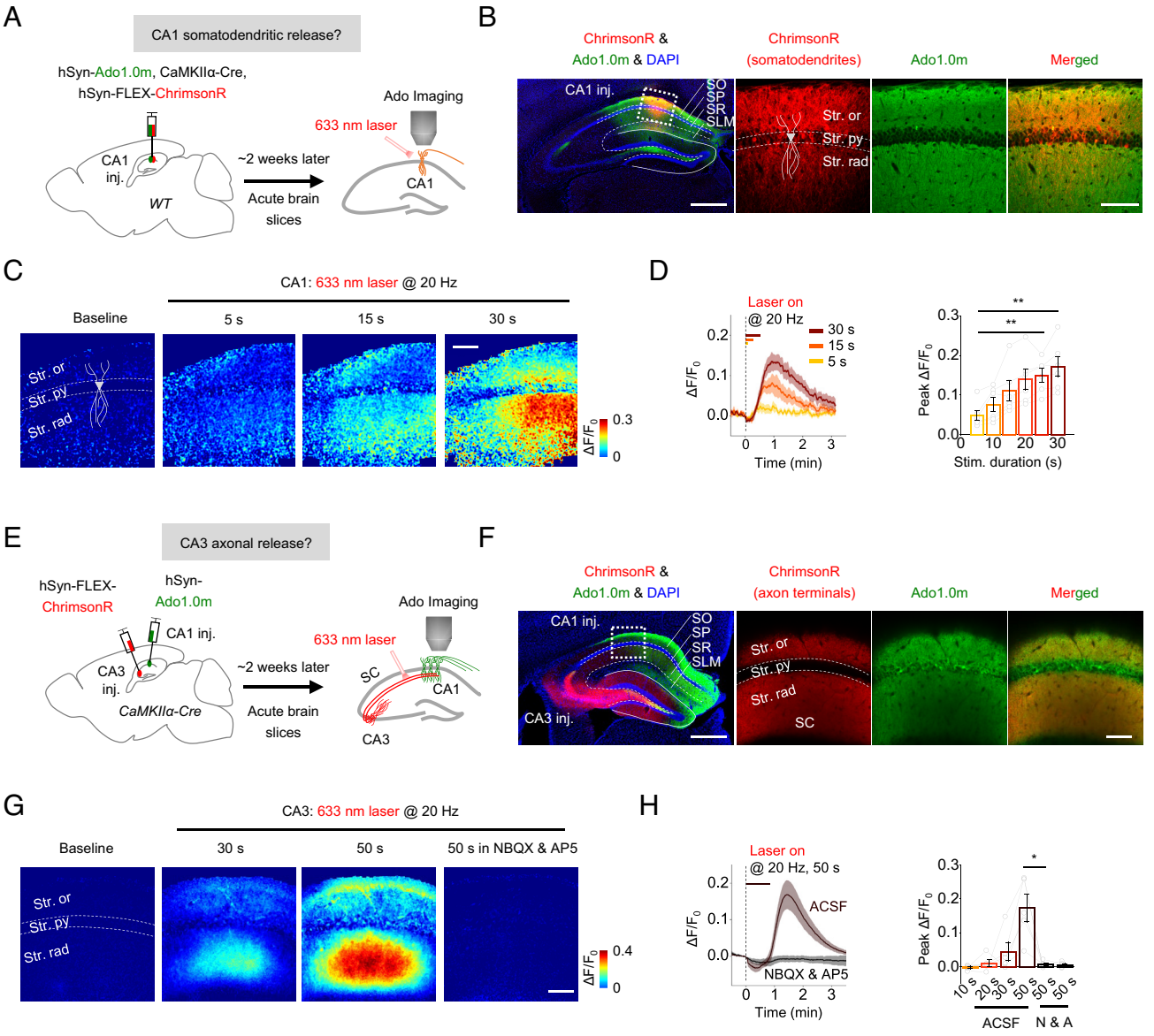

Fig. 2. $GRAB_{Ado}$ reveals somatodendritic Ado release in the hippocampus. (*A*) Schematic illustration depicting the strategy used to image acute hippocampal brain slices prepared from mice expressing Ado1.0m and ChrimsonR-mCherry in the CA1 region while using a 633-nm laser to activate the neurons. (*B*) *Left*, Fluorescence images of hippocampus showing the expression of Ado1.0m (green) and ChrimsonR (red). *Right*, magnified fluorescence images of the CA1 region show ChrimsonR-mCherry and Ado1.0m in CA1 regions. The pyramidal cell layer (Str. py, SP) is located between the stratum oriens (Str. ori, SO) and stratum radiatum (Str. rad, SR). Stratum Lacunosum Moleculare (SLM). (*C* and *D*) Pseudocolor images (*C*), traces, and group summary (*D*) of Ado1.0m $\Delta F/F_0$ in response to 633-nm laser pulses applied at 20 Hz for the indicated duration; n = 6 slices from four mice. (*E*) Schematic illustration depicting the strategy used to image acute hippocampal brain slices prepared from mice expressing Ado1.0m in the CA1 region and ChrimsonR-mCherry in the CA3 region while using a 633-nm laser to activate the axonal terminals (Schaffer Collaterals, SC) in the CA1 region. (*F*) *Left*, a fluorescence image of the hippocampus showing the expression of Ado1.0m (green) and ChrimsonR-mCherry (red). *Right*, large magnification of fluorescence images showing ChrimsonR-mCherry and Ado1.0m din CA1 regions. (*G* and *H*) Pseudocolor images (*G*), traces, and group summary (*H*) of Ado1.0m $\Delta F/F_0$ in response to 633-nm laser pulses applied at 20 Hz for the indicated duration in the absence (ACSF) and presence of 10 μM NBQX and 50 μM D-AP5 (N & A); after adding N & A, 633-nm laser pulses were applied twice at 20 Hz for 50 s; n = 5 slices from two mice. (Scale bars represent 500 μm [*B* and *F*, *Left*] and 100 μm [others].) Summary data are presented as the mean ± SEM; statistical significance in (*D*) was assessed using a one-way ANOVA followed by Bonferroni's multiple comparison test; statistical significance in (*H*) was assessed using Student's *t* test; $^{**}P < 0.01$; $^{*}P < 0.05$. See also *SI Appendix*, Figs. S4 and S5.

Ado1.0 fluorescence; meanwhile, there was no detectable increase in Ado1.0mut control fluorescence (*SI Appendix*, Fig. S6 *A–D*), suggesting the specificity of the signal. Notably, we found a transient decrease in Ado1.0 fluorescence in the presence of ZM-241385, SCH-58261, or Ado1.0mut-expressed neurons following the onset of stimulation (*SI Appendix*, Fig. S6), likely caused by the neuronal activity-associated intracellular pH changes as previously reported (21). Moreover, increasing the duration of stimulation at 30 Hz caused progressively stronger responses (*SI Appendix*, Fig. S7 *A* and *B*).

After confirming that we could reliably record Ado release in cultures, we next expressed Ado1.0 and mjRGECO1a in the same cultures for simultaneous dual-color imaging of Ado release and neuronal Ca^{2+} activities. Blocking action potential firing with tetrodotoxin (TTX) prevented the electrical stimuli–induced increase in Ado1.0 and mjRGECO1a fluorescence (Fig. 3 *E–G*), suggesting that the observed Ado release was neuronal activity-dependent. We examined whether the neuronal activity–induced Ado release required Ca^{2+} signaling by applying cadmium (Cd^{2+}), a nonselective blocker of voltage-gated Ca^{2+} channels (VGCCs). We simultaneously

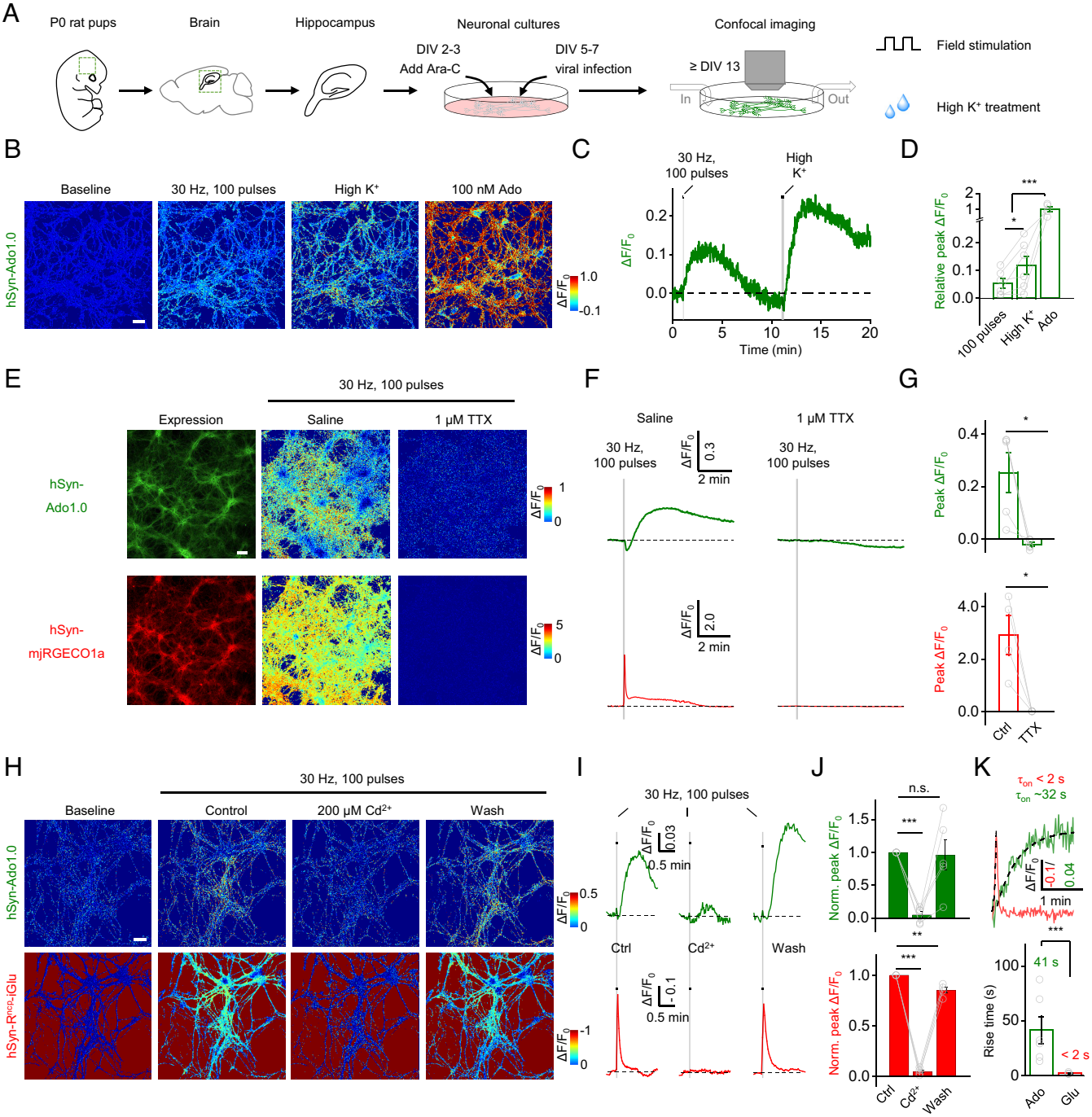

Fig. 3. Neuronal activity and Ca^{2+}-dependent Ado release in hippocampal cultures. (*A*) Schematic diagram depicting the experimental protocol in which primary hippocampal neurons are cultured and infected with an AAV encoding Ado1.0 and GAP43-jRGECO1a / R^{ncp}-iGluSnFR under the control of the hSyn promoter, followed by confocal fluorescence microscopy during field stimuli or high K^+ treatment. Ara-C, cytosine β-D-arabinofuranoside, inhibits glial proliferation; DIV, days in vitro. (*B–D*) Ado1.0-expressing cultured hippocampal neurons were stimulated with 100 field stimuli at 30 Hz, high K^+, or 100 nM Ado. Exemplar pseudocolor images (*B*), example traces (*C*), and summary data (*D*) are shown; in this and subsequent panels, n = 4 to 6 coverslips each. (*E–G*) Dual-color imaging of Ado1.0 (*Upper*) and mjRGECO1a (*Bottom*) in response to 100 field stimuli at 30 Hz applied before and during bath application of 1 μM TTX. Exemplar pseudocolor images (*E*), traces (*F*), and summary data (*G*) are shown; in this and subsequent panels, n = 4 to 5 coverslips each. (*H–J*) Dual-color imaging of Ado1.0 (*Upper*) and R^{ncp}-iGlu (*Bottom*) in response to 100 field stimuli at 30 Hz applied before (control), during, and after (wash) bath application of 200 μM Cd^{2+}. Exemplar pseudocolor images (*H*), exemplar traces (*I*), and summary data (*J*) are shown; n = 4 to 5 coverslips. (*K*) Exemplar traces (*Top*) and summary data (*Bottom*) showing the kinetics of Ado1.0 and R^{ncp}-iGlu $\Delta F/F_0$; n = 4 to 6 coverslips. (Scale bars represent 30 μm.) Summary data are presented as the mean ± SEM; statistical significance was assessed using Student's *t* test; ***$P < 0.001$; **$P < 0.01$; *$P < 0.05$; n.s., not significant. See also *SI Appendix*, Figs. S6–S8.

imaged glutamate (Glu) and Ado signals by coexpressing the red fluorescent Glu sensor R^{ncp}-iGluSnFR (R^{ncp}-iGlu) (22) and the green fluorescent Ado1.0 sensor in neurons. As expected, stimuli-evoked Glu release was blocked by Cd^{2+} (Fig. 3 *H–J*) and recovered after wash. Moreover, the Cd^{2+} application also blocked Ado1.0 responses (Fig. 3 *H–J*), suggesting that Ca^{2+} influx through VGCCs is required for electrical stimulation–induced Ado release. Next, we determined that the rise-time constants were ~41 s and <2 s for stimulation-induced Ado and Glu release, respectively (Fig. 3*K*). The slow on-kinetics of the Ado signal was likely due to the slow release of Ado but not the sensor's intrinsic kinetics, given that Ado1.0 can rapidly respond to extracellular Ado with

68 ms on-rate (18). Taken together, we found that Ado could release in a neuronal activity- and VGCC-dependent manner, with long-lasting releasing properties.

Next, we examined the contribution of astrocytes on Ado release. In hippocampal astrocyte cultures, none of the stimuli tested—including electrical field stimulation (30 Hz, 100 pulses), high K^+, glutamate (100 μM), bradykinin (1 μM), and thrombin (30 nM) application—induced significant fluorescence signals in Ado1.0. However, glutamate, bradykinin, and thrombin evoked robust intracellular Ca^{2+} responses in the astrocytes (*SI Appendix*, Fig. S8 *A–F*), as reported previously (23, 24). Furthermore, we expressed hM3Dq-DREADD under the control of GfaABC1D promoter in mice (*SI Appendix*, Fig. S8 *G* and *H*) and monitored Ado release in acute brain slices. The application of Clozapine N-oxide (CNO) did not induce a detectable increase in fluorescence signals of the Ado sensor (*SI Appendix*, Fig. S8 *I–K*). At the same time, GCaMP6s imaging confirmed that CNO successfully activated the astrocytes (*SI Appendix*, Fig. S8 *L–N*). These results suggest that neuronal activation represents the main source of Ado release in the hippocampus.

Equilibrative Nucleoside Transporters (ENTs) Mediate the Activity-Dependent Release of Ado. The relatively slow release of Ado suggests that this process is unlikely mediated by synaptic vesicle fusion, which is a rapid process (25). To validate this, we expressed the tetanus toxin light chain (TeNT), which cleaves synaptobrevin and prevents exocytosis (26, 27). As expected, neurons expressing TeNT abolished stimulation-evoked Glu release; in contrast, Ado release showed no detectable effects (Fig. 4 *A–D*), suggesting that the release of Ado from neurons did not require synaptobrevin-dependent vesicle fusion. We next examined whether the degradation of extracellular ATP mediates the Ado1.0 signal. Pharmacologically blocking CD39 or genetically deleting CD73, the two critical ectoenzymes for the ATP/ADP to Ado conversion, did not show detectable effects on field electrical stimulation–induced Ado1.0 signals, suggesting that extracellular ATP had minimal contributions to the neuronal activity–induced extracellular Ado increase in cultured hippocampal neurons (Fig. 4 *E–G*).

We then examined whether ENTs mediate neuronal activity–induced Ado release (Fig. 4*H*). Application of the ENT inhibitors S-(4-nitrobenzyl)-6-thioinosine (NBTI, 5 μM) and dipyridamole (DIPY, 10 μM) reversibly inhibited high K^+-induced Ado release but not Glu release (Fig. 4 *H–J*), indicating that the ENT activity is required for activity-induced Ado release in hippocampal neurons. ENT1 and ENT2 are the major nucleoside transporters that control extracellular Ado levels, and both are expressed in the hippocampus (28, 29). We used pharmacological and genetic approaches to examine their contributions. The application of 5 μM NBTI, a more selective ENT1 inhibitor (30), blocked ~65% of Ado release induced by field stimulation. A mixture of 5 μM NBTI and 10 μM DIPY, which inhibited both ENT1 and ENT2, abolished Ado release (*SI Appendix*, Fig. S9). These results suggested that both ENT1 and ENT2 contribute to activity-dependent Ado release. We further substantiated the conclusion by generating ENT1 and ENT2 knockout mice using the CRISPR-Cas9 strategy. ENT1 homozygous knockout or ENT2 homozygous knockout only partially blocked neuronal activity–induced Ado release (Fig. 4 *N* and *O*). Since ENT1 and ENT2 double knockout mice fail to survive during the early postnatal period, we used SaCas9-mediated manipulations (31) to ablate ENT1 expression in cultured hippocampal neurons from ENT2 knockout mice (Fig. 4 *K* and *L*). Immunoblots showed that SaCas9-sgENT1 robustly induced suppression of ENT1-HA protein levels (Fig. 4*M*). Ado1.0 imaging demonstrated that the ENT1 deletion in ENT2 knockout mice (ENT2 KO & sgENT1 KO) effectively eliminated neuronal activity–induced Ado release (Fig. 4 *N* and *O*). Thus, the pharmacological and genetic experiments suggested that ENT transporters are required for neuronal activity–induced Ado release.

The Ca^{2+} Source Mediating Activity-Induced Ado Release. Given that ENT transporters mediate the Ado release but not classical vesicular machinery, we then study which Ca^{2+} sources are essential for the Ado release. In neurons, Ca^{2+} entry through VGCCs, which are activated by membrane depolarization and trigger neurotransmitter release. P/Q-type and N-type VGCCs inactivate rapidly and initiate neurotransmitter release at most fast synapses (32–34). L-type VGCCs have slow voltage-dependent inactivation and are long-lasting (35, 36). Given the striking kinetics differences between neuronal glutamate and adenosine releases, it is possible that they couple with distinct Ca^{2+} signaling, e.g., different subtypes of VGCCs (Fig. 5*A*). To dissect the roles of various VGCC subtypes, we used specific blockers and simultaneously monitored glutamate and Ado release from the same neurons. Electrical stimulation–induced Ado release was inhibited by nimodipine (Fig. 5 *B* and *C*) and felodipine (*SI Appendix*, Fig. S10*A*), which block L-type VGCCs, the channel subtype primarily localized at the somatodendritic membrane in neurons (37, 38), including CA1 neurons (38, 39). Conversely, Ado release was slightly decreased by blocking P/Q-type and N-type VGCCs with ω-Conotoxin-GVIA and ω-Agatoxin-IVA (Fig. 5 *B* and *C* and *SI Appendix*, Fig. S10*B*), which are predominantly localized to presynaptic terminals and dictate Glu release (40) (Fig. 5 *B* and *C*). The failure to completely block Ado release by the two VGCC channel inhibitors likely arises from the fact that field electrical stimulation could induce Ca^{2+} influx through other VGCCs, such as the L-type VGCCs. We also noticed that when we blocked P/Q-type, followed by N-type and L-type VGCCs, Ado, and glutamate release showed a similar tendency, suggesting that the sequence of blocking different VGCCs might affect the Ado release with different proportions. Together, these data are consistent with the finding that the activity-induced Ado release occurs primarily in the somatodendritic region.

To quantify the relative Ca^{2+} sensitivity of both Ado and Glu release in the same neurons, we measured the fluorescence responses of Ado1.0 and R^{ncp}-iGlu as a function of external Ca^{2+} concentration (*SI Appendix*, Fig. S7*C*). Ado1.0 and R^{ncp}-iGlu fluorescence were imaged while applying electrical stimuli (100 pulses at 30 Hz) at increasing extracellular Ca^{2+} (ranging from 0.25 to 4 mM, *SI Appendix*, Fig. S7*D*). We then normalized the response measured at each Ca^{2+} concentration to the response measured at 4 mM Ca^{2+} and generated Ca^{2+}-dose–response curves (*SI Appendix*, Fig. S7*E*). To calculate the apparent affinity for extracellular Ca^{2+}, the dose–response curve was fitted with the following Hill function: $(\Delta F/F_0 = 1/(1+(EC_{50}/[Ca^{2+}])^n)$ as previously reported (41, 42), where $\Delta F/F_0$ is the normalized Ado1.0 or R^{ncp}-iGlu response, EC_{50} is the apparent dissociation constant for extracellular Ca^{2+}, $[Ca^{2+}]$ is the extracellular Ca^{2+} concentration, and n is the apparent cooperativity (or Hill coefficient). Interestingly, we found that the calculated Ca^{2+} affinity was lower for Ado release than for Glu release, with apparent EC_{50} values of 1.16 mM and 0.46 mM, respectively; moreover, the cooperativity of Ado release was slightly lower than for Glu release, with Hill coefficient values of 1.91 and 2.11, respectively (*SI Appendix*, Fig. S7*E*). These results indicate that activity-induced Ado release requires more Ca^{2+} than that Glu release.

We also tested whether triggering Ca^{2+} release from internal Ca^{2+} stores (by activating Gq-coupled GPCRs at the cell membrane)

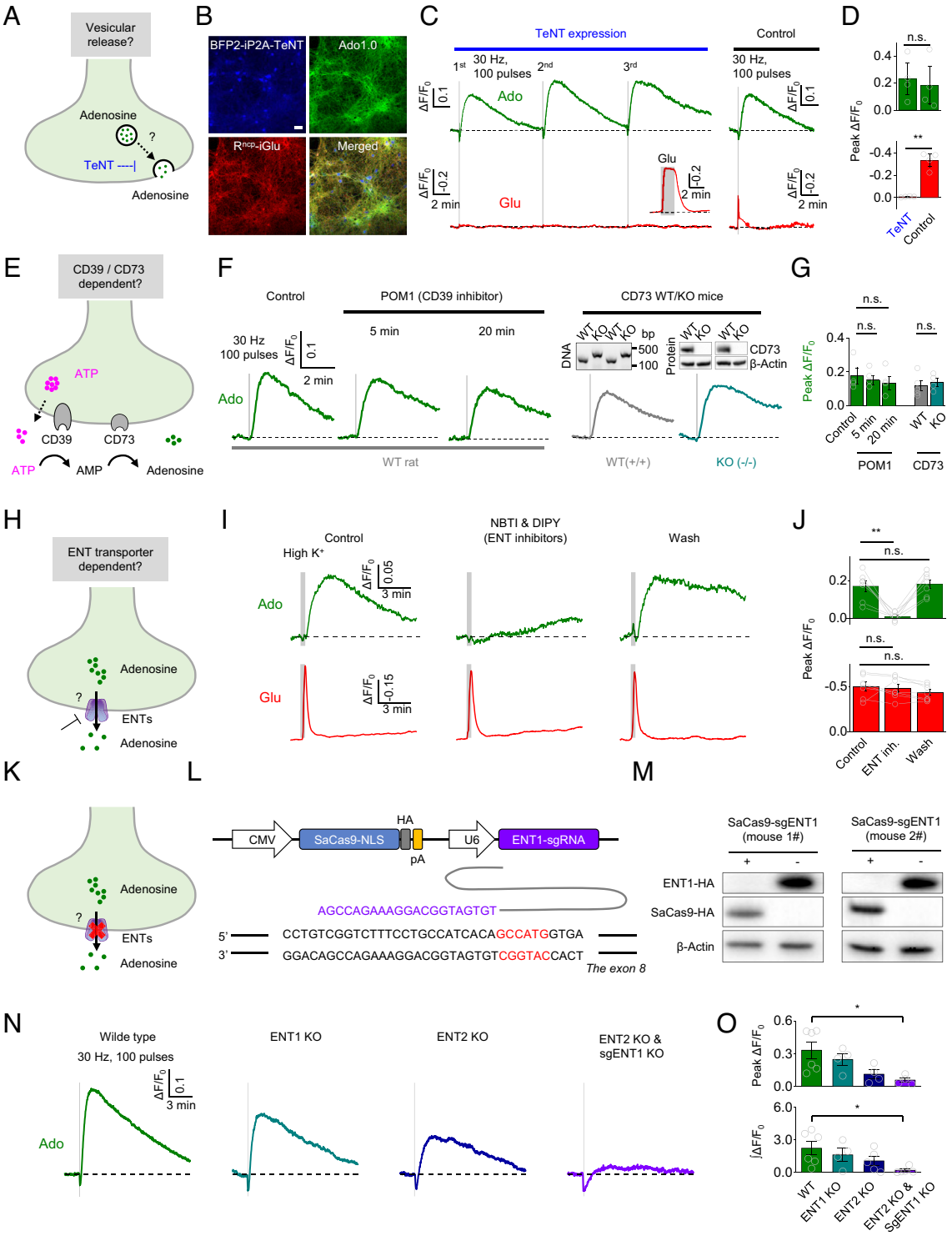

Fig. 4. ENT transporters mediated Ado release in hippocampal cultures. (*A–D*) Blocking synaptic vesicle release with tetanus neurotoxin (TeNT) abolishes glutamate release but not Ado release. (*A*) Schematic drawing depicting the release of neurotransmitter-containing synaptic vesicles, which are blocked by TeNT. (*B*) Representative confocal images showing hippocampal neurons expressing TeNT (blue), Ado1.0 (green), and R^{ncp}-iGlu (red). (*C* and *D*) Exemplar traces (*C*) and group summary (*D*) of Ado1.0 (*Upper* panels, green) and R^{ncp}-iGlu (*Bottom* panels, red) $\Delta F/F_0$ in response to field stimuli (30 Hz, 100 pulses) with or without TeNT expression; n = 4 coverslips per group. (*E–G*) Blocking CD39 or knocking out CD73 does not affect activity-dependent Ado release. (*E*) Schematic drawing depicting the production of Ado from ATP via the CD39 and CD73 enzymes. (*F* and *G*) Traces (*F*) and group summary (*G*) of Ado1.0 $\Delta F/F_0$ in response to field stimuli (30 Hz, 100 pulses) under control conditions, in the presence of the CD39 inhibitor POM1 (10 μM), and in CD73 knockout neurons; n = 4 to 5 coverslips per group. The *Inset* in (*F*) shows an example of PCR genotyping and western blotting results of CD73 KO mice. (*H–J*) Pharmacological inhibition of ENTs blocks activity-dependent Ado release but not glutamate release. (*H*) Schematic drawing depicting the release of Ado via ENTs. (*I* and *J*) Traces (*H*) and group summary (*J*) of Ado1.0 (*Upper* panels, green) and R^{ncp}-iGlu (*Bottom* panels, red) $\Delta F/F_0$ in response to high K^+ before (control), during, and after (wash) application of NBTI (5 μM) and DIPY (10 μM); n = 7 coverslips each. (*K–O*) Knockout ENTs block activity-dependent Ado release. (*K*) Schematic drawing depicting the release of Ado via ENTs. (*L*) The design of sgRNAs for ENT1. (*M*) Immunoblots showing SaCas9-induced suppression of ENT1 protein levels. (*N* and *O*) Traces (N) and group summary (*O*) of Ado1.0 $\Delta F/F_0$ in response to 30 Hz, 100 pulses in cultured hippocampal neurons from wild-type (WT) mice, ENT1 knockout mice, ENT2 knockout mice, and ENT1/2 double knockout (ENT2 KO & sgENT1 KO) mice; n = 4 to 6 coverslips. The scale bar represents 100 μm. Summary data are presented as the mean ± SEM; statistical significance was assessed using Student's *t* test; $^{**}P < 0.01$; $^{*}P < 0.05$; n.s., not significant. See also *SI Appendix*, Fig. S9.

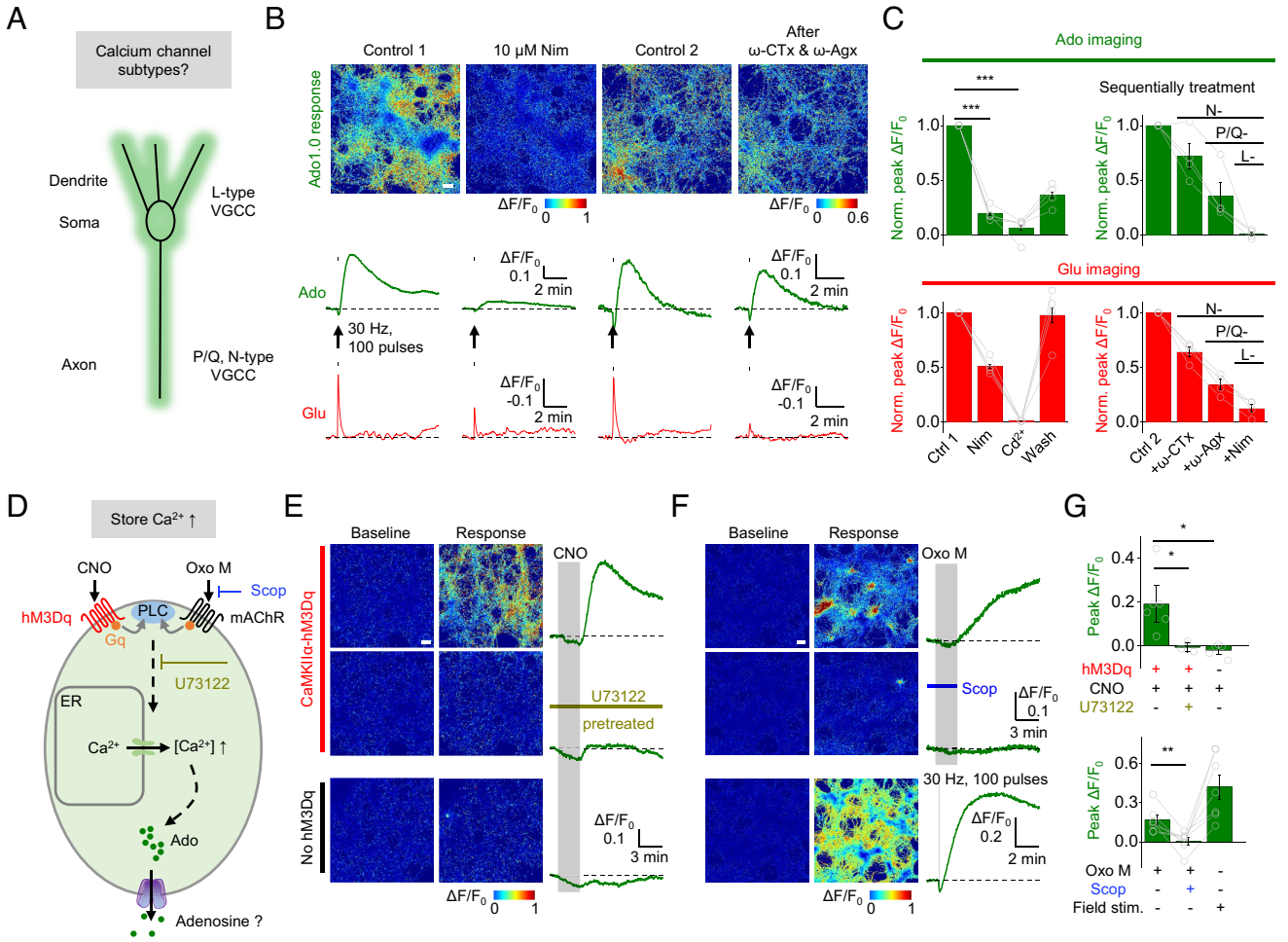

Fig. 5. Dissecting the Ca^{2+} source that mediates activity-dependent Ado release. (*A–C*) Activity-dependent Ado release is blocked by inhibitors of L-type voltage-gated calcium channels (VGCCs). (*A*) Schematic drawing depicting the expression of various VGCC subtypes in specific neuronal compartments. (*B*) Pseudocolor images (*Upper*) and exemplar traces (*Lower*) of Ado1.0 and R^{ncp}-iGlu $\Delta F/F_0$ in response to field stimuli (30 Hz, 100 pulses) applied before (control), during, and after (wash) application of nimodipine (Nim, 10 μM) or Cd^{2+} (200 μM). (*C*) Group summary of Ado1.0 (green) and R^{ncp}-iGlu (red) $\Delta F/F_0$ in response to field stimuli, measured in the presence of Cd^{2+} (200 μM) or Nim (10 μM), ω-Conotoxin-GVIA (ω-CTx, 1 μM), and ω-Agatoxin-IVA (ω-Agx, 0.3 μM) to block L-type, N-type, and P/Q-type VGCCs respectively; n = 4 coverslips each. (*D–G*) Activation of Gq-coupled GPCRs induces Ado release. (*D*) Schematic drawing depicting the experimental strategy. CNO and oxotremorine-M (Oxo-M) were used to activate recombinant hM3Dq-mCherry and endogenous Gq-coupled mAChRs, respectively; where indicated, the mAChR antagonist scopolamine (Scop) or the phospholipase C inhibitor U73122 was applied. (*E*) Pseudocolor images (*Left*) and example traces (*Right*) of Ado1.0 $\Delta F/F_0$ in CaMKIIα-hM3Dq-expressing neurons in response to CNO (5 μM) in the absence (*Top*) or presence (*Middle*) of U73122 (10 μM); shown below are neurons that do not express CaMKIIα-hM3Dq. (*F*) Pseudocolor images (*Left*) and example traces (*Right*) of Ado1.0 $\Delta F/F_0$ in response to Oxo-M (10 μM) in the absence (*Top*) or presence (*Middle*) of Scop (1 μM); as a positive control, separate neurons were stimulated with 100 pulses at 30 Hz (*Bottom*). (*G*) Summary of Ado1.0 $\Delta F/F_0$ measured under the indicated conditions; n = 3 to 7 coverslips. (Scale bars represent 100 μm.) Summary data are presented as the mean ± SEM. Statistical significance was assessed using Student's *t* test; ***$P < 0.001$; **$P < 0.01$; *$P < 0.05$. See also *SI Appendix*, Figs. S7 and S10.

can induce Ado release (Fig. 5*D*). Activating the Gq-coupled signaling pathway chemogenetically or activating the endogenous metabotropic acetylcholine receptors triggered Ado release (Fig. 5 *E–G*, and *SI Appendix*, Fig. S10*C*). The release was blocked by pretreating the cells with the phospholipase inhibitor U73122 (10 μM) and the mAChR antagonist scopolamine (1 μM), respectively (Fig. 5 *E–G*). Based on these results, we conclude that both depolarization-induced Ca^{2+} influx through L-type VGCCs and Ca^{2+} release from intracellular stores can drive Ado release from hippocampal neurons.

ENT Transporters Mediated Somatodendritic Ado Release in Hippocampal Slices. Having identified that the neuronal-activity–dependent Ado release is mediated by ENTs and requires L-type VGCCs in cultures, we next asked whether Ado's somatodendritic release also needs L-type VGCCs and ENTs in acute hippocampal slices. Inhibiting L-type VGCCs with nimodipine significantly attenuated optogenetic stimuli (20 Hz, 20s) induced Ado release at CA1 somatodendritic compartments (Fig. 6 *A–C* and *SI Appendix*, Fig. S11 *A–D*), adding Cd^{2+} further reduced Ado release. Consistent with the results in cultured hippocampal neurons, blocking CD73 with α,β-Methyleneadenosine 5′-diphosphate (AMP-CP, 10 μM) in acute brain slices did not significantly suppress the optogenetic stimuli induced Ado release (*SI Appendix*, Fig. S11 *E* and *F*). To investigate the ENTs' contributions, we used the pharmacological method to inhibit ENTs. We found that the ENTs inhibitor DIPY significantly attenuated Ado release at CA1 (Fig. 6 *D* and *E*). Moreover, we used SaCas9-mediated manipulations to ablate ENT1 expression in ENT1 heterogeneous and ENT2 homozygous knockout mice. Again, the genetic deletion of ENT transporters also significantly attenuated the activity-induced release of Ado at CA1 (Fig. 6 *F–I*), consistent with the findings in cultured hippocampal neurons. Thus, we concluded that the somatodendritic release of Ado at CA1 required L-type VGCCs and ENTs transporters.

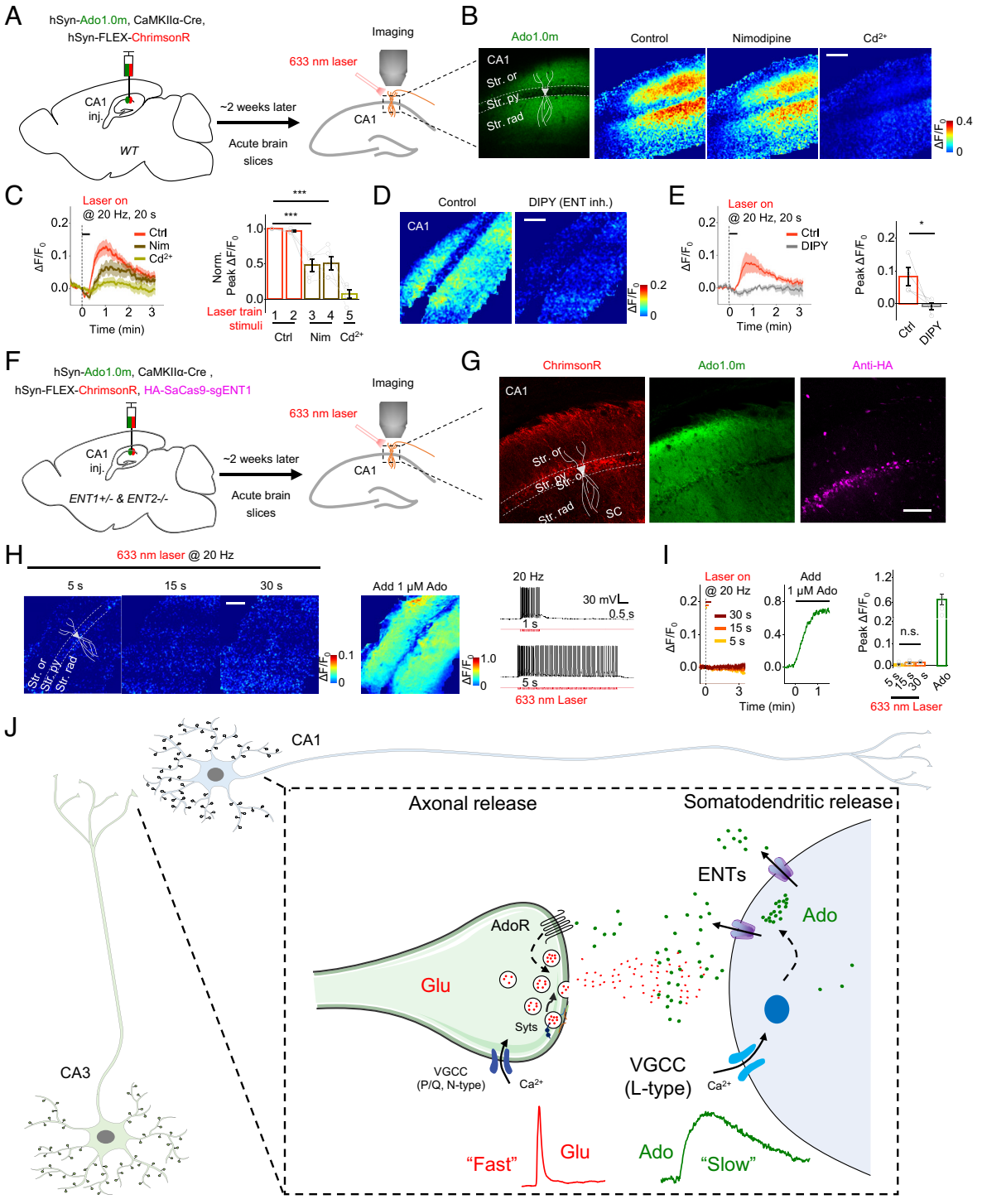

Fig. 6. ENT-dependent somatodendritic Ado release in hippocampal slices. (*A*) Schematic illustration depicting the strategy used to image acute hippocampal brain slices prepared from mice expressing Ado1.0m and ChrimsonR-tdTomato in the CA1 region while using a 633-nm laser to activate the neurons. (*B* and *C*) Blocking L-type VGCCs inhibits optogenetically induced Ado release. Images (*B*), traces, and group summary (*C*) of Ado1.0m $\Delta F/F_0$ in response to 633-nm laser pulses applied at 20 Hz for the indicated duration; where indicated, nimodipine (Nim, 20 μM) and Cd^{2+} (100 μM) were applied (Scale bar, 100 μm); n = 5 slices from three mice. (*D* and *E*) Pharmacological blockade of ENT transporters inhibits optogenetically induced Ado release. Where indicated, DIPY (20 μM) was used to block ENTs. Images (*D*), traces, and group summary (*E*) of Ado1.0m $\Delta F/F_0$ are shown; n = 4 slices from three mice. (*F–I*) Knockout of ENT transporters inhibits optogenetically induced Ado release. (*F*) Schematic illustration depicting the strategy used to image acute hippocampal brain slices prepared from ENT2−/− & ENT1+/− mice expressing Ado1.0m, ChrimsonR-tdTomato, and HA-SaCas9-sgENT1 in the CA1 region while using a 633-nm laser to activate the neurons. (*G*) Fluorescence images of the CA1 region showing Ado1.0m (green), ChrimsonR-tdTomato (red), and HA-SaCas9 (purple) in CA1 regions. (*H* and *I*) Pseudocolor images (*H*), traces, and the group summary (*I*) of Ado1.0m $\Delta F/F_0$ in response to 633-nm laser pulses applied at 20 Hz for the indicated duration, n = 6 slices from three mice; the right traces in (*H*) show electrophysiological recordings at ChrimsonR-expressing CA1 neurons while using a 633-nm laser to activate the neurons. (*J*) Model depicting the novel mode of neuronal activity-dependent Ado release from hippocampal neurons. Ado is released slowly from the postsynaptic membrane via a vesicle-independent, ENT-dependent mechanism, serving as a putative retrograde signal to regulate presynaptic activity. This activity-dependent release of Ado requires L-type VGCCs. In contrast, classic neurotransmitters such as glutamate (Glu) are released from presynaptic vesicles that require P/Q-type and N-type VGCCs. AdoR, adenosine receptor; ENTs; Syts, synaptotagmins. (Scale bars represent 100 μm.) Summary data are presented as the mean ± SEM. The data in (*E*) were analyzed using Student's *t* test; the data in (*C*) and (*I*) were analyzed using a one-way ANOVA followed by Bonferroni's multiple comparison test; ***$P < 0.001$; *$P < 0.05$; n.s., not significant. See also *SI Appendix*, Fig. S11.

Discussion

Here, we unraveled pathways and mechanisms that regulate the neuronal activity–induced release of Ado by capitalizing on the newly developed and further optimized genetically encoded adenosine fluorescent sensor, $GRAB_{Ado}$. As illustrated by the model (Fig. 6*J*), we find that in the hippocampal CA1 region, Ado is released slowly from the postsynaptic membrane via a vesicle-independent, ENT-dependent mechanism, serving as a putative retrograde signal to regulate presynaptic activity. This activity-dependent release of Ado requires L-type VGCCs. In contrast, classical neurotransmitters such as glutamate (Glu) are released from presynaptic vesicles that require P/Q-type and N-type VGCCs.

Concerning the site of Ado release in CA1, intracellular loading of Ado to an individual hippocampal CA1 pyramidal neuron was reported to inhibit excitatory postsynaptic potentials, suggesting that Ado is capable of being released from the somatodendritic compartments (11). Here, we found that the activity-induced release of endogenous Ado was mainly from somatodendritic compartments of CA1 neurons but not CA3 axonal terminals (Fig. 2). Consistently, the activity-dependent Ado release was very sensitive to blockers for L-type VGCC (Figs. 5 *A*–*C* and 6 *A*–*C*), a subtype known to be primarily localized at the somatodendritic region (38, 39). A recent study identified the Ado/A_{2A} receptor as a retrograde signaling system that mediates presynaptic long-term potentiation on mossy cells to granule cell synapses, suggesting the potential functions of Ado as a retrograde signal (43). Given the abundance of presynaptic A_1/A_{2A} receptors and Ado's known presynaptic inhibition function in distinct brain regions (11, 44, 45), our work suggests the somatodendritic release of Ado could serve as a retrograde modulator to feedback control presynaptic release.

The Ado release is blocked when voltage-dependent Na^+ channels (Fig. 3 *E*–*G*) or VGCCs are blocked (Fig. 3 *H*–*J*), which supports the conclusion that neurons are the predominant source for Ado release following electrical and optogenetic stimulations (8, 14). Furthermore, no detectable Ca^{2+}-dependent Ado release is observed in cultured astrocytes and acute brain slices from the hippocampus, which is consistent with a recent finding that astrocytes have a minor contribution to Ado release during sleep-wake cycles in the basal forebrain (46). Nevertheless, we cannot exclude the possibility that glial cells can also release Ado or ATP under other conditions (9, 47, 48), such as astrocytic Ado release can reduce synaptic neurotransmitter release during hypoxia (9). We also cannot exclude the contribution of CD73 conversion in the other brain regions, like the striatum (49, 50). In this respect, the new $GRAB_{Ado}$ and $GRAB_{ATP}$ sensors (51) may serve as valuable tools for examining this possibility in the future.

What are the molecular mechanisms underlying Ado release? Using $GRAB_{Ado}$ sensors combined with a spectrally distinct glutamate sensor, we found that the kinetics of Ado release was much slower than the vesicular release of glutamate from the same neurons (Fig. 3*K*). Importantly, we found that pharmacological or genetic inhibition of ENT transporters, but not exocytosis machinery, abolished the Ado release without affecting glutamate release (Fig. 4). In the same neurons, depolarization-induced Ado release required higher extracellular Ca^{2+} than glutamate release (*SI Appendix*, Fig. S7), suggesting different Ca^{2+} dependencies for Ado and glutamate. We also notice that 20 pulses at different frequencies caused a comparable amount of Ado release (*SI Appendix*, Fig. S2 *A*–*D*), the underlying mechanism of which is unclear and may need further study.

Our data reveal unique routes and molecular pathways that control Ado release, which differs from the conventional vesicular- and SNARE-dependent pathways for classic neurotransmitters, such as glutamate. Given that Ado is not only an extracellular neuromodulator but also an intracellular homeostatic modulator, the intracellular ATP/Ado levels may be regulated during neuronal activities (52, 53). It remains unclear whether Ca^{2+} elevation is required to generate intracellular Ado, the Ado transportation through ENTs, or both. Since both the extracellular Ca^{2+} and intracellular Ca^{2+} can induce the Ado release, it is possible that the Ca^{2+}-ATPases may involve because Ca^{2+}-ATPases may elevate the intracellular Ado from the hydrolysis of ATP. The availability of a comprehensive GRAB toolbox for purinergic transmitters (16), combined with robust emerging techniques such as optogenetic/chemogenetic and CRISPR/Cas9, may provide new tools for studying the roles and mechanisms of purinergic transmission in both physiological and pathological conditions.

Materials and Methods

Molecular Biology. Plasmids were generated using Gibson assembly (54). DNA fragments were generated using PCR amplification with primers (Tsingke) with ~25-bp overlap, and all sequences were verified using Sanger sequencing. The plasmids used to express the $GRAB_{Ado}$ sensors in neurons or astrocytes were cloned into the pAAV vector using the human synapsin promoter (hSyn) or GfaABC1D promoter. The membrane-targeted jRGECO1a (mjRGECO1a) was cloned by fusing an N-terminus of growth-associated protein-43 (GAP43) (55) to jRGECO1a (56), as previously reported (57). The plasmid encoding the glutamate sensor R^{ncp}-iGluSnFR (22) was a gift from Dr. Robert Campbell (The University of Tokyo), and the plasmid encoding TeNT was a gift from Dr. Peng Cao (National Institute of Biological Sciences). The pX601 plasmid (Addgene #61591) was kindly provided by Dr. Feng Zhang (Massachusetts Institute of Technology). Three sgRNAs targeting *SLC29A1* (*ENT1*, 5′- GGCAGTGACAAGGAATACCAG-, 5′ -GCCAACTACACAGCCCCCATC-, and 5′- TTGAGCTGCAGGTAATGGCGA) were designed using the web tool Benchling (https://benchling.com/crispr) and subsequently synthesized and cloned into the original pX601 plasmids following the SaCas9 user manual (31); three plasmids were purified, respectively, and mixed for AAV preparation.

Cell Cultures. Details are given in *SI Appendix*.

Mice. All animals were family- or pair-housed in a temperature-controlled room with a 12-h/12-h light/dark cycle. All animal surgery and maintenance protocols were approved by the Animal Care and Use Committees at Peking University, the Chinese Academy of Sciences, and the National Institute of Biological Sciences. They were performed following the guidelines established by the U.S. NIH. Both male and female mice (P0 pups for primary neuron cultures and adults >6 wk for acute slices and in vivo experiments) were used for experiments. Nt5e (CD73) knockout mice (JAX Strain 018986) and CaMKIIα-Cre (JAX Strain 005359) mice were obtained from Jackson Laboratory. ENT1 knockout mice, ENT2 knockout mice, and ENT1-HA knock-in mice were created using CRISPR/Cas9 technology by Beijing Biocytogen.

AAV Virus Preparation. The following AAV viruses were used to infect cultured neurons and for *in vivo* expression: AAV2/9-hSyn-Ado1.0, AAV2/9-GfaABC1D-Ado1.0, AAV2/9-hSyn-Ado1.0mut, AAV2/9-hSyn-GAP43-jRGECO1a, AAV2/9-hSyn-R^{ncp}-iGluSnFR, AAV2/9-hSyn-Ado1.0m, AAV2/9-CAG-EBFP2-iP2A-TeNT, and AAV2/9-CMV-SaCas9-sgENT1 (packaged at Vigene Biosciences Shandong); AAV2/9-CaMKIIα-hM3Dq-mCherry and AAV2/9-GfaABC1D-NES-jRGECO1a (packaged at BrainVTA Wuhan); AAV2/9-CaMKIIα-Cre, AAV2/9-hSyn-FLEX-ChrimsonR-mCherry or tdTomato, AAV2/8-GfaABC1D-hM3Dq-mCherry, and AAV2/9-CAG-FLEX-jGCaMP7s (packaged at Shanghai Taitool Bioscience).

Expression of $GRAB_{Ado}$ in Cultured Cells and In Vivo. HEK293T cells were transfected at 50 to 60% confluency with a mixture of polyethyleneimine (PEI) and plasmid DNA at a 3:1 (w/w) ratio; after 6 to 8 h, the transfection reagent was replaced with standard culture medium, and the cells were cultured for an additional 24 to 36 h for expression of the transfected plasmids.

For in vitro expression in cultured neurons, the viruses were added to cultured neurons at days in vitro DIV) 5 to 7 and characterized ≥48 h after infection. For physiological analyses, DIV ≥13 neurons were used.

For in vivo expression, adult (>6 wk of age) mice were anesthetized either with isoflurane (RWD Life Science) inhalation or Avertin (500 mg/kg, Sigma, i.p. injection), placed in a stereotaxic frame, and AAVs were injected using a microsyringe pump (Nanoliter 2000 Injector, WPI).

For examining the knockout efficiency of AAV2/9-SaCas9-sgENT1 in adult ENT1-HA knock-in mice, we injected the virus unilaterally into the posterior thalamic nucleus, which exhibits a high expression level of ENT1 according to the Allen Brain Atlas (54). We used the following coordinates: A.P.: −2.2 mm relative to Bregma, ML: −1.5 mm relative to Bregma, and DV: 3.4 mm below the dura.

Confocal Imaging of $GRAB_{Ado}$ in Cultured Cells. To screen the medium affinity adenosine sensor, HEK293T cells were imaged using an Opera Phenix High-Content Screening System (PerkinElmer).

$GRAB_{Ado}$-expressing cultured neurons were imaged using a Ti-E A1 inverted confocal microscope (Nikon). For confocal imaging, the microscope was equipped with either a 20×/0.75 NA objective or a 10×/0.5 NA objective, a 405-nm laser, a 488-nm laser, and a 561-nm laser. A 450/25-nm, a 525/50-nm, and a 595/50-nm emission filter were used to collect the BFP, GFP, and RFP signals, respectively. $GRAB_{Ado}$-expressing HEK293T cells or neurons were perfused with Tyrode's solutions containing the drug of interest in the imaging chamber. The cultured cells were bathed or perfused during imaging in a chamber with Tyrode's solution.

For field stimulation, neurons were stimulated using platinum electrodes as previously described (58); except where indicated otherwise, the stimulation voltage was set at 80 V, and the duration of each stimulation pulse was typically set at 1 ms. All experiments were performed at room temperature.

More details are given in *SI Appendix*.

Preparation and Fluorescence Imaging of Acute Brain Slices. Wild-type adult (6 to 12 wk) C57BL/6N mice or CaMKIIα-Cre mice were anesthetized with an intraperitoneal injection of Avertin (500 mg/kg body weight) and placed in a stereotaxic frame for AAV injection using a microsyringe pump (Nanoliter 2000 Injector, WPI). AAVs were injected into the hippocampal CA3 region using the following coordinates: A.P.: −1.80 mm, ML: ±2.2 mm, and DV: −1.80 mm. AAVs were injected into the hippocampal CA1 region using the following coordinates: A.P.: −1.8 mm, ML: ±1.0 mm, and DV: −1.5 mm. For the data in Fig. 1 *G–J* and *SI Appendix*, Fig. S1, AAVs expressing hSyn-Ado1.0m were injected into the mPFC region using the following coordinates: A.P.: +1.78 mm, ML: ±0.25 mm, and DV: −2.4 mm.

Two to four weeks after virus injection, the mice were anesthetized with an intraperitoneal (i.p.) injection of Avertin (500 mg/kg body weight) and perfused with ice-cold oxygenated slicing buffer containing (in mM): 110 choline chloride, 2.5 KCl, 0.5 $CaCl_2$, 7 $MgCl_2$, 1.3 NaH_2PO_4, 25 $NaHCO_3$, 20 glucose, 1.3 Na-ascorbate, and 0.6 Na-pyruvate. The brains were immediately removed and placed in an ice-cold oxygenated slicing buffer. The brains were then sectioned into 200-μm thick slices using a VT1200 vibratome (Leica). The slices were incubated at 34 °C for at least 40 min in oxygenated artificial cerebrospinal fluid (ACSF) containing (in mM) 125 NaCl, 2.5 KCl, 2 $CaCl_2$, 1.3 $MgCl_2$, 1.3 NaH_2PO_4, 1.3 Na-ascorbate, 0.6 Na-pyruvate, 20 glucose, and 25 $NaHCO_3$.

The slices were transferred to an imaging chamber for fluorescence imaging and placed under an FV1000MPE 2-photon microscope (Olympus) equipped with a 20× water-immersion objective and a mode-locked Mai Tai Ti: Sapphire laser (Spectra-Physics). A 488-nm laser was used to excite Ado1.0m, and fluorescence was collected using a 495 to 540-nm filter. For electrical stimulation, a bipolar electrode (cat. number WE30031.0A3, MicroProbes for Life Science) was positioned near the CA1 stratum radiatum using fluorescence guidance. Fluorescence imaging and electrical stimulation were synchronized using an Arduino board with custom-written programs. All images collected during electrical stimulation were recorded at 1.3 frames/s, with 320 × 320 pixels per frame. For photostimulation, an optical fiber (200 μm core diameter, NA = 0.22) coupled to a diode-pumped solid-state 633-nm laser was submerged in ACSF and placed ~500 μm from the imaging region.

For immunofluorescence staining in brain slices, details are given in *SI Appendix*.

Patch-Clamp Electrophysiology. Details are given in *SI Appendix*.

Western Blotting. Details are given in *SI Appendix*.

Data Analysis. Image data from cell cultures and acute brain slices were first processed with ImageJ software (NIH), traces were generated by Origin2019 (OriginLab), and pseudocolor images were generated by ImageJ. The fluorescence responses ($\Delta F/F_0$) were calculated as $(F_{raw}-F_{baseline})/F_{baseline}$.

We used Origin2019 and GraphPad Prism 5 (GraphPad) to perform the statistical analysis. Sample sizes (n) were reported in figure captions and figure legends. Except where indicated otherwise, groups were analyzed using either Student's *t* test or the one-way ANOVA. Unless indicated otherwise, summary data are presented as the mean ± SEM.

Data, Materials, and Software Availability. The plasmids for expressing Ado1.0m used in this study have been deposited at Addgene (Addgene Plasmid ID 153292, 153289 and 153286). All study data are included in the article and/or *SI Appendix*.

ACKNOWLEDGMENTS. We thank the members of the Li lab for their suggestions and comments; we thank Drs. J.-F. Chen, M.-M. Poo, P. Castillo, J.-T. Lv, and Y.-H. Huang for critical reading of the manuscript; we thank Dr. Y.-S. Shu for the scientific discussion. This work was supported by grants from National Natural Science Foundation of ChinaNSFC (92032000 and 31925017 to Y.L., 31871074 to M.X., 91432114 and 91632302 to M.L.); the Beijing Municipal Science & Technology Commission (Z181100001318002 and Z181100001518004 to Y.L.); the "Strategic Priority Research Program" of the Chinese Academy of Sciences (XDB32010000 to M.X.); National Key R&D Program of China (2017YFE0196600 to M.X.); the China Ministry of Science and Technology (2015BAI08B02 to M.L.); the Research Unit of Medical Neurobiology at Chinese Academy of Medical Sciences (2019RU003 to M.L.); New Cornerstone Investigator Program (to M.L. and Y.L.) the Beijing Municipal Government (to M.L.); and STI2030-Major Projects (2022ZD0208300 to Z.W.). Z.W. is supported by the Young Elite Scientists Sponsorship Program by Beijing Association for Science and Technology, the Boehringer Ingelheim-Peking University Postdoctoral Program and Postdoctoral Fellowship of Peking-Tsinghua Center for Life Sciences.

Author affiliations: [a]State Key Laboratory of Membrane Biology, School of Life Sciences, Peking University, Beijing 100871, China; [b]IDG/McGovern Institute for Brain Research, Peking University, Beijing 100871, China; [c]Peking-Tsinghua Center for Life Sciences, Academy for Advanced Interdisciplinary Studies, Peking University, Beijing 100871, China; [d]National Institute of Biological Sciences, Beijing 102206, China; [e]Chinese Institute for Brain Research, Beijing 102206, China; [f]School of Life Sciences, Tsinghua University, Beijing 100084, China; [g]Peking University-Tsinghua University-National Institute of Biological Sciences Joint Graduate Program, Peking University, Beijing 100871, China; [h]Institute of Neuroscience, State Key Laboratory of Neuroscience, Center for Excellence in Brain Science and Intelligence Technology, Chinese Academy of Sciences, Shanghai 200031, China; [i]Tsinghua Institute of Multidisciplinary Biomedical Research, Tsinghua University, Beijing 102206, China; [j]Research Unit of Medical Neurobiology, Chinese Academy of Medical Sciences, Beijing 100005, China; [k]New Cornerstone Science Institute at Chinese Institute for Brain Research, Beijing 102206, China; [l]Institute of Molecular Physiology, Shenzhen Bay Laboratory, Shenzhen, Guangdong 518055, China; [m]National Biomedical Imaging Center, Peking University, Beijing 100871, China; and [n]New Cornerstone Science Institute at Peking University, Beijing 100871, China

1. A. Drury, A. V. Szent-Györgyi, The physiological activity of adenine compounds with especial reference to their action upon the mammalian heart 1. *J. Physiol.* **68**, 213–237 (1929).
2. J.-F. Chen, H. K. Eltzschig, B. B. Fredholm, Adenosine receptors as drug targets–what are the challenges? *Nat. Rev. Drug Discov.* **12**, 265 (2013).
3. R. B. Dias, D. M. Rombo, J. A. Ribeiro, J. M. Henley, A. M. Sebastiao, Adenosine: Setting the stage for plasticity. *Trends Neurosci.* **36**, 248–257 (2013).
4. T. V. Dunwiddie, The physiological role of adenosine in the central nervous system. *Int. Rev. Neurobiol.* **27**, 63–139 (1985).
5. G. Hasko, J. Linden, B. Cronstein, P. Pacher, Adenosine receptors: Therapeutic aspects for inflammatory and immune diseases. *Nat. Rev. Drug Discov.* **7**, 759–770 (2008).
6. N. Dale, B. G. Frenguelli, Release of adenosine and ATP during ischemia and epilepsy. *Curr. Neuropharmacol.* **7**, 160–179 (2009).
7. R. A. Cunha, How does adenosine control neuronal dysfunction and neurodegeneration. *J. Neurochem.* **139**, 1019–1055 (2016).
8. D. Lovatt *et al.*, Neuronal adenosine release, and not astrocytic ATP release, mediates feedback inhibition of excitatory activity. *Proc. Natl. Acad. Sci. U.S.A.* **109**, 6265–6270 (2012).
9. E. D. Martín *et al.*, Adenosine released by astrocytes contributes to hypoxia-induced modulation of synaptic transmission. *Glia* **55**, 36–45 (2007).
10. P. Schubert, K. Lee, M. West, S. A. Deadwyler, G. Lynch, Stimulation-dependent release of 3H-adenosine derivatives from central axon terminals to target neurones. *Nature* **260**, 541–542 (1976).
11. J. M. Brundege, T. V. Dunwiddie, Modulation of Excitatory Synaptic Transmission by Adenosine Released from Single Hippocampal Pyramidal Neurons. *J. Neurosci.* **16**, 5603–5612 (1996).

12. G. Burnstock, Purinergic signalling and disorders of the central nervous system. *Nat. Rev. Drug Discov* **7**, 575 (2008).
13. M. J. Wall, N. Dale, Neuronal transporter and astrocytic ATP exocytosis underlie activity-dependent adenosine release in the hippocampus. *J. Physiol.* **591**, 3853–3871 (2013).
14. J. M. Brundege, T. V. Dunwiddie, Metabolic regulation of endogenous adenosine release from single neurons. *Neuroreport* **9**, 3007–3011 (1998).
15. F. Corti *et al.*, Adenosine is present in rat brain synaptic vesicles. *Neuroreport* **24**, 982–987 (2013).
16. Z. Wu, Y. Li, New frontiers in probing the dynamics of purinergic transmitters in vivo. *Neurosci. Res.* **152**, 35–43 (2020).
17. M. D. Nguyen, B. J. Venton, Fast-scan Cyclic Voltammetry for the Characterization of Rapid Adenosine Release. *Comput. Struct. Biotechnol. J.* **13**, 47–54 (2015).
18. W. Peng *et al.*, Regulation of sleep homeostasis mediator adenosine by basal forebrain glutamatergic neurons. *Science* **369** (2020).
19. B. N. Cronstein, M. Sitkovsky, Adenosine and adenosine receptors in the pathogenesis and treatment of rheumatic diseases. *Nat. Rev. Rheumatol.* **13**, 41–51 (2017).
20. B. B. Fredholm, Adenosine, an endogenous distress signal, modulates tissue damage and repair. *Cell Death & Differentiation* **14**, 1315–1323 (2007).
21. Z. Zhang, K. T. Nguyen, E. F. Barrett, G. David, Vesicular ATPase inserted into the plasma membrane of motor terminals by exocytosis alkalinizes cytosolic pH and facilitates endocytosis. *Neuron* **68**, 1097–1108 (2010).
22. J. Wu *et al.*, Genetically encoded glutamate indicators with altered color and topology. *ACS Chem. Biol.* **13**, 1832–1837 (2018).
23. V. Parpura *et al.*, Glutamate-mediated astrocyte-neuron signalling. *Nature* **369**, 744–747 (1994).
24. C. J. Lee *et al.*, Astrocytic control of synaptic NMDA receptors. *J. Phys.* **581**, 1057–1081 (2007).
25. T. C. Sudhof, Neurotransmitter release: The last millisecond in the life of a synaptic vesicle. *Neuron* **80**, 675–690 (2013).
26. G. G. Schiavo *et al.*, Tetanus and botulinum-B neurotoxins block neurotransmitter release by proteolytic cleavage of synaptobrevin. *Nature* **359**, 832 (1992).
27. M. Patterson, E. Szatmari, R. Yasuda, AMPA receptors are exocytosed in stimulated spines and adjacent dendrites in a Ras-ERK–dependent manner during long-term potentiation. *Proc. Natl. Acad. Sci. U.S.A.* **107**, 15951–15956 (2010).
28. K. C. Wu, C. Y. Lee, F. Y. Chou, Y. Chern, C. J. Lin, Deletion of equilibrative nucleoside transporter-2 protects against lipopolysaccharide-induced neuroinflammation and blood-brain barrier dysfunction in mice. *Brain Behav. Immun.* **84**, 59–71 (2020).
29. C. M. Anderson *et al.*, Distribution of equilibrative, nitrobenzylthioinosine-sensitive nucleoside transporters (ENT1) in brain. *J. Neurochem.* **73**, 867–873 (1999).
30. J. L. Ward, A. Sherali, Z. P. Mo, C. M. Tse, Kinetic and pharmacological properties of cloned human equilibrative nucleoside transporters, ENT1 and ENT2, stably expressed in nucleoside transporter-deficient PK15 cells. Ent2 exhibits a low affinity for guanosine and cytidine but a high affinity for inosine. *J. Biol. Chem.* **275**, 8375–8381 (2000).
31. F. A. Ran *et al.*, In vivo genome editing using Staphylococcus aureus Cas9. *Nature* **520**, 186–191 (2015).
32. K. Dunlap, J. I. Luebke, T. J. Turner, Exocytotic Ca2+ channels in mammalian central neurons. *Trends Neurosci.* **18**, 89–98 (1995).
33. W. A. Catterall, Structure and regulation of voltage-gated Ca2+ channels. *Annu. Rev. Cell Dev. Biol.* **16**, 521–555 (2000).
34. B. M. Olivera, G. P. Miljanich, J. Ramachandran, M. E. Adams, Calcium channel diversity and neurotransmitter release: The omega-conotoxins and omega-agatoxins. *Annu. Rev. Biochem.* **63**, 823–867 (1994).
35. R. W. Tsien, D. Lipscombe, D. V. Madison, K. R. Bley, A. P. Fox, Multiple types of neuronal calcium channels and their selective modulation. *Trends Neurosci.* **11**, 431–438 (1988).
36. M. C. Nowycky, A. P. Fox, R. W. Tsien, Three types of neuronal calcium channel with different calcium agonist sensitivity. *Nature* **316**, 440–443 (1985).
37. H. Vacher, D. P. Mohapatra, J. S. Trimmer, Localization and targeting of voltage-dependent ion channels in mammalian central neurons. *Phys. Rev.* **88**, 1407–1447 (2008).
38. J. W. Hell *et al.*, Identification and differential subcellular localization of the neuronal class C and class D L-type calcium channel alpha 1 subunits. *J. Cell Biol.* **123**, 949–962 (1993).
39. B. Leitch, A. Szostek, R. Lin, O. Shevtsova, Subcellular distribution of L-type calcium channel subtypes in rat hippocampal neurons. *Neuroscience* **164**, 641–657 (2009).
40. D. B. Wheeler, A. D. Randall, R. W. Tsien, Roles of N-type and Q-type Ca2+ channels in supporting hippocampal synaptic transmission*Science* **264**, 107–111 (1994).
41. F. A. Dodge, R. Rahamimoff, Co-operative action of calcium ions in transmitter release at the neuromuscular junction. *J. Physiol.* **193**, 419–432 (1967).
42. R. Fernandezchacon *et al.*, Synaptotagmin I functions as a calcium regulator of release probability. *Nature* **410**, 41–49 (2001).
43. K. Nasrallah, Retrograde adenosine/A2A receptor signaling mediates presynaptic hippocampal LTP and facilitates epileptic seizures. *bioRxiv* (2021), https://doi.org/10.1101/2021.10.07.463512.
44. O. J. Manzoni, T. Manabe, R. A. Nicoll, Release of adenosine by activation of NMDA receptors in the hippocampus. *Science* **265**, 2098–2101 (1994).
45. D. Brambilla, D. Chapman, R. W. Greene, Adenosine mediation of presynaptic feedback inhibition of glutamate release. *Neuron* **46**, 275–283 (2005).
46. W. Peng *et al.*, Adenosine-independent regulation of the sleep–wake cycle by astrocyte activity. *Cell Discovery* **9**, 16 (2023).
47. M. M. Halassa *et al.*, Astrocytic modulation of sleep homeostasis and cognitive consequences of sleep loss. *Neuron* **61**, 213–219 (2009).
48. Y. Li *et al.*, Activation of astrocytes in hippocampus decreases fear memory through adenosine A1 receptors. *Elife* **9**, e57155 (2020).
49. F. Q. Gonçalves *et al.*, Increased ATP Release and higher impact of adenosine A2A receptors on corticostriatal plasticity in a rat model of presymptomatic Parkinson's disease. *Mol. Neurobiol.* **60**, 1659–1674 (2022), 10.1007/s12035-022-03162-1.
50. L. Ma *et al.*, Locomotion activates PKA through dopamine and adenosine in striatal neurons. *Nature* **611**, 762-+ (2022).
51. Z. Wu *et al.*, A sensitive GRAB sensor for detecting extracellular ATP in vitro and in vivo. *Neuron* **110**, 770–782.e775 (2022).
52. R. A. Cunha, Adenosine as a neuromodulator and as a homeostatic regulator in the nervous system: Different roles, different sources and different receptors. *Neurochem. Int.* **38**, 107–125 (2001).
53. R. A. Cunha, How does adenosine control neuronal dysfunction and neurodegeneration? *J. Neurochem.* **139**, 1019–1055 (2016).
54. D. G. Gibson *et al.*, Enzymatic assembly of DNA molecules up to several hundred kilobases. *Nat. Methods* **6**, 343–345 (2009).
55. A.E.-D. El-Husseini, S. E. Craven, S. C. Brock, D. S. Bredt, Polarized targeting of peripheral membrane proteins in neurons. *J. Biol. Chem.* **276**, 44984–44992 (2001).
56. H. Dana *et al.*, Sensitive red protein calcium indicators for imaging neural activity. *Elife* **5**, e12727 (2016).
57. G. J. Broussard *et al.*, In vivo measurement of afferent activity with axon-specific calcium imaging. *Nat. Neurosci.* **21**, 1272–1280 (2018).
58. Y. Li, R. W. Tsien, pHTomato, a red, genetically encoded indicator that enables multiplex interrogation of synaptic activity. *Nat. Neurosci.* **15**, 1047 (2012).

PNAS

Supplementary Information for

Neuronal activity-induced, equilibrative nucleoside transporter-dependent, somatodendritic adenosine release revealed by a GRAB sensor

Zhaofa Wu[a,b,c,1], Yuting Cui[d,e,1], Huan Wang[a,b,1], Hao Wu[f], Yi Wan[a,b,c], Bohan Li[a,b,c], Lei Wang[a,b,g], Sunlei Pan[a,b,c], Wanling Peng[h], Ao Dong[a,b,c], Zhengwei Yuan[d,f], Miao Jing[e], Min Xu[h], Minmin Luo[d,e,i,j,k,2], and Yulong Li[a,b,c,l,m,n,2]

[1] Z.W., Y.C. and Huan W. contributed equally to this work.

[2] Corresponding authors: Minmin Luo and Yulong Li

Email: luominmin@nibs.ac.cn (M.L.); yulongli@pku.edu.cn (Y.L.)

This PDF file includes:

Supplementary materials and methods
Supplemental Fig 1-11

Supplementary materials and methods

Cell cultures

HEK293T cells were obtained from ATCC (CRL-3216) and verified based on their morphology under the microscope and by their growth curve. HEK293T cells were cultured at 37°C in 5% CO2 in DMEM (Biological Industries) supplemented with 10% (v/v) fetal bovine serum (FBS, CellMax) and 1% (v/v) penicillin-streptomycin (Gibco).

Rat and mouse primary neurons were prepared from 0-day-old (P0) pups (male and female, randomly selected). Hippocampal neurons were dissociated from the dissected brains in 0.25% Trypsin-EDTA (Gibco) and plated on 12-mm glass coverslips coated with poly-D-lysine (1mg/ml, Sigma-Aldrich) in a neurobasal medium (GIBCO) containing 2% B-27 supplement (Gibco), 1% (v/v) GlutaMAX (Gibco), and 1% penicillin-streptomycin (Gibco). Based on glial cell density, after approximately 3 days in culture (DIV 3), cytosine β-D-arabinofuranoside (Sigma) was added to the hippocampal cultures in a 50% growth media exchange at a final concentration of 2 μM.

Primary astrocytes were prepared as previously described (1). In brief, the hippocampi were dissected from P0 rat pups, and the cells were dissociated with trypsin digestion for 10 mins at 37ºC and plated on a poly-D-lysine-coated T25 flask. The plating and culture media contained DMEM supplemented with 10% (v/v) FBS and 1% penicillin-streptomycin. The next day and every 2 days thereafter, the medium was changed. At DIV 7-8, the flask was shaken on an orbital shaker at 180 rpm for 30 min, and the supernatant containing the microglia was discarded; 10 ml of fresh astrocyte culture medium was then added to the flask, which was shaken at 240 rpm for ≥6 h to remove oligodendrocyte precursor cells. The remaining astrocytes were dissociated with trypsin and plated on 12-mm glass coverslips containing culture medium.

Chemicals and drugs

Adenosine (Sigma), adenosine 5'-triphosphate (ATP, sigma), SCH-58261 (Abcam), ZM-241385 (MedChemExpress or Bio-Techne), NBQX (Sigma), D-AP5 (Tocris or MedChemExpress), tetrodotoxin (TTX, absin), $CdCl_2$ (Sigma), POM1 (Santa Cruz), S-(4-nitrobenzyl)-6-thioinosine (NBTI, Santa Cruz), dipyridamole (Santa Cruz), ω-Conotoxin-GVIA (Tocris), ω-Agatoxin IVA (Cayman), Clozapine N-oxide (CNO, Cayman), nimodipine (Cayman), (±)-felodipine (Cayman), oxotremorine-M (Oxo-M, Cayman), Scopolamine (Tocris), U73122 (Tocris), L-glutamate (Sigma), bradykinin (Sangon Biotech Shanghai), and thrombin (Sigma).

Confocal imaging in cultured cells

Solutions containing chemicals or drugs were delivered via a custom-made perfusion system or bath application. The chamber was cleaned thoroughly with Tyrode's solution and 75% ethanol between experiments. The GFP signal ($GRAB_{Ado}$ sensors) was collected using a 525/50-nm emission filter, and the RFP signal (GAP43-jRGECO1a, jRGECO1a, R^{ncp}-iGluSnFR, mCherry, and Calbryte 590,) was collected using a 595/50-nm emission filter, and the BFP signal (EBFP2-iP2A-TeNT) was recorded using a 450/25-nm emission filter. Where applicable, cells were pre-loaded

with the Ca^{2+} dye Calbryte 590-AM (AAT Bio) by incubation at 37ºC for 40 min before imaging. High K^+-containing Tyrode's solution contained (in mM): 79 NaCl, 75 KCl, 2 $MgCl_2$, 2 $CaCl_2$, 10 HEPES, and 10 glucose (pH 7.3-7.4).

Immunofluorescence staining in brain slices

Brains were fixed in 4% PFA for 8 h at room temperature and dehydrated in 30% sucrose solution for 1~2 days. Thin sections (30 μm) were prepared on a freezing microtome (Leica CM1950). Slices were permeabilized in PBS with 0.3% Triton X-100 (PBST) and blocked in 5% BSA in PBST at room temperature for 40 min. Slices were incubated with primary antibodies (anti-HA, 1:1000, #3724, Cell Signaling Technology) at 4°C overnight. Slices were washed three times in PBST and then incubated with fluorescent secondary antibodies (goat anti-rabbit Alexa Fluor 647, 1:500, 111-605-144, Jackson ImmunoResearch Labs) at room temperature for 2 h and then washed three times in PBST. Brain slices were imaged using Zeiss LSM800.

Patch-clamp electrophysiology

For Patch-clamp electrophysiology, the brain slices were transferred to a recording chamber at room temperature for recordings. The cell was identified with differential interference contrast optics. The pipettes (2-6 MΩ) used for the recordings were prepared using a micropipette puller (P1000, Sutter Instrument). For whole-cell recordings, the pipettes were filled with an internal solution that contained the following (mM): 130 K-gluconate, 10 HEPES, 0.6 EGTA, 5 KCl, 3 Na.2ATP, 0.3 Na.3GTP, 4 MgCl2, and 10 Na.2-phosphocreatine. Voltage- and current-clamp recordings were performed with a MultiClamp 700B amplifier (Molecular Devices). The neurons were held at −65 mV. For photostimulation, an optical fiber (200 μm core diameter, NA = 0.22) coupled to a diode-pumped solid-state 633 nm laser was submerged in ACSF and placed ∼500 μm from the recording site. Data were acquired and analyzed using Clampfit 10.0 software (Molecular Devices).

Western blotting

Tissue samples were collected from mice brains. Tissue lysates were prepared in SA buffer (in mM): 20 HEPES; 10 KCl, 1.5 $MgCl_2$, 1 EDTA, 1 EGTA, 2 DTT, and 0.3% (w/v) Chaps with EDTA-free protease inhibitor cocktail (Roche). After denaturation (70 ℃, 10 min), samples were separated on SDS-polyacrylamide gels (prepared through SDS-PAGE Gel Kit, CWBIO) for 30 min at 90 V and 50 min at 140V, then transferred to a hybridization nitrocellulose transfer membrane (Millipore) for 2 h at 200 mA. The solution of 5% non-fat milk (APPLYGEN) in TBST was used for blocking (1 h at room temperature) and subsequent primary antibody incubations (4 ℃, overnight). Anti-HA-tag (rabbit, CST), anti-CD73 (Abclonal), and anti-β-actin (mouse, CWBIO) was used in western blot.

References

1. S. Schildge, C. Bohrer, K. Beck, C. Schachtrup, Isolation and culture of mouse cortical astrocytes. JoVE, e50079 (2013).

SI Appendix Fig. S1

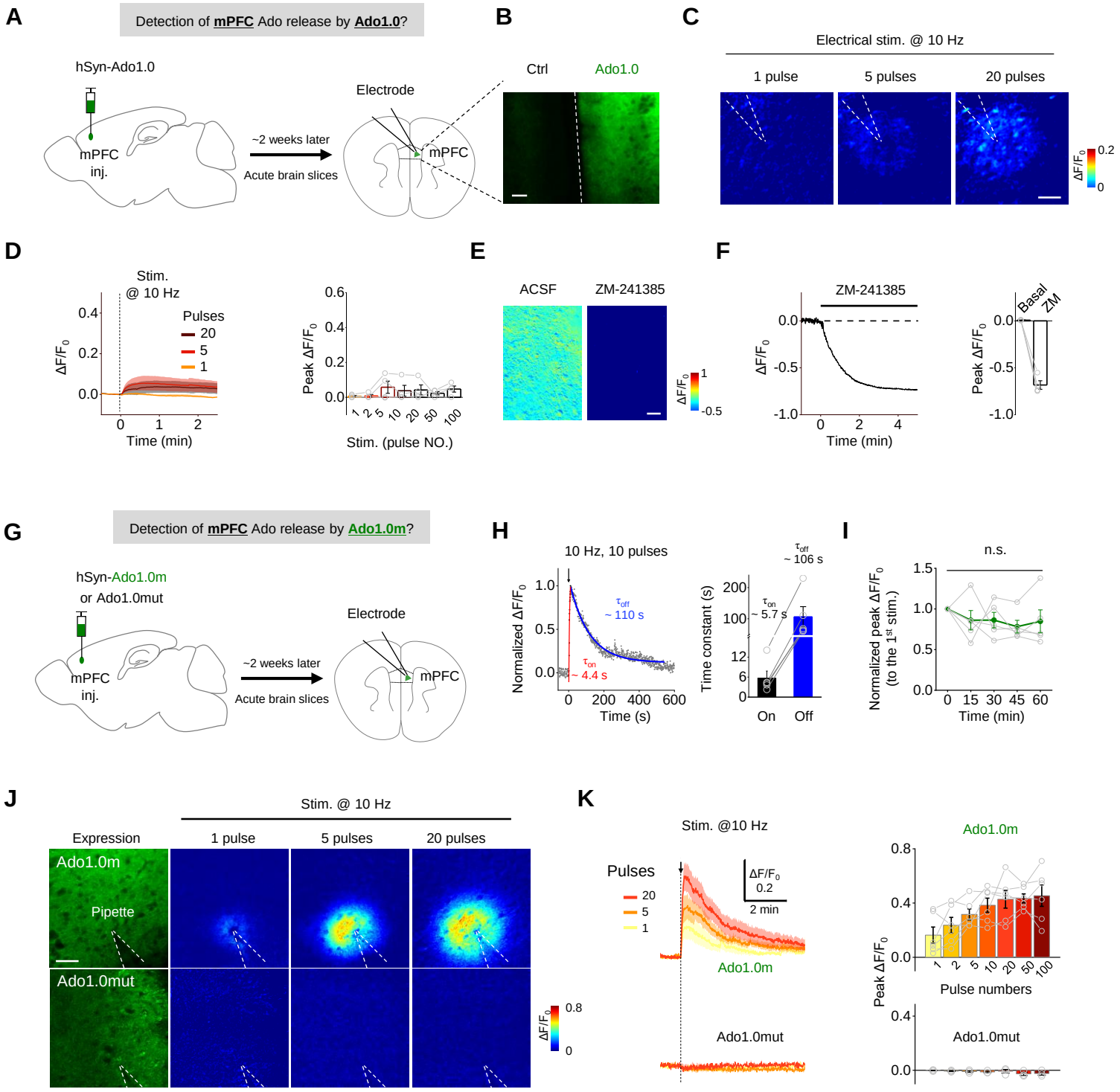

Fig. S1. The characterization of Ado1.0 and Ado1.0m in acute mPFC brain slices, related to Fig. 1.

(A-F) Detecting Ado release with Ado1.0 in the mPFC.

(A) Schematic illustration depicting the expression of Ado1.0 in the mouse mPFC, an acute brain slice containing the mPFC, and the placement of a bipolar stimulating electrode in the mPFC.

(B) Fluorescence images showing the expression of Ado1.0 in the ipsilateral mPFC, with no expression in the contralateral mPFC.

(C) Pseudocolor images of Ado1.0 $\Delta F/F_0$ in response to 1, 5, and 20 electrical pulses at 10 Hz.

(D) Traces (left panels) and group summary (right panels) of Ado1.0 $\Delta F/F_0$ in response to 1, 5, and 20 electrical pulses at 10 Hz; n = 4 slices from 3 mice each.

(E) Pseudocolor images of Ado1.0 $\Delta F/F_0$ in response to control solution (ACSF) or solution containing the $A_{2A}R$ antagonist ZM-241385 (1 μM).

(F) Traces (left panels) and group summary (right panels) of Ado1.0 $\Delta F/F_0$ in control solution (ACSF) or solution containing the $A_{2A}R$ antagonist ZM-241385 (ZM, 1 μM); n = 4 slices from 3 mice.

(G-K) Detecting Ado release with Ado1.0m in the mPFC.

(G) Schematic illustration depicting the expression of Ado1.0m or Ado1.0mut in the mouse mPFC.

(H) Representative traces (left) and group summary (right) of normalized $\Delta F/F_0$ and kinetics (τ_{on} and τ_{off}) in Ado1.0m-expressing neurons in response to 10 electrical stimuli delivered at 10 Hz; n = 5 slices from 3 mice.

(I) $\Delta F/F_0$ was measured in Ado1.0m-expressing neurons in response to repeated trains of electrical stimuli applied every ~15 min and normalized to the first train; n = 5 slices from 4 mice.

(J) Fluorescent images of Ado1.0m- or Ado1.0mut-expressing in the mPFC (left panels) and pseudocolor images of Ado1.0m and Ado1.0mut $\Delta F/F_0$ in response to the indicated number of electrical stimuli delivered at 10 Hz (right panels).

(K) Example traces and group summary of Ado1.0m and Ado1.0mut $\Delta F/F_0$ in response to the indicated number of electrical stimuli delivered at 10 Hz; n = 6 slices from 3 mice per group.

Scale bars represent 50 μm. Summary data are presented as the mean ± SEM. Statistical significance in **(I)** was assessed using a one-way ANOVA followed by Bonferroni's Multiple Comparison Test; n.s. not significant.

SI Appendix Fig. S2

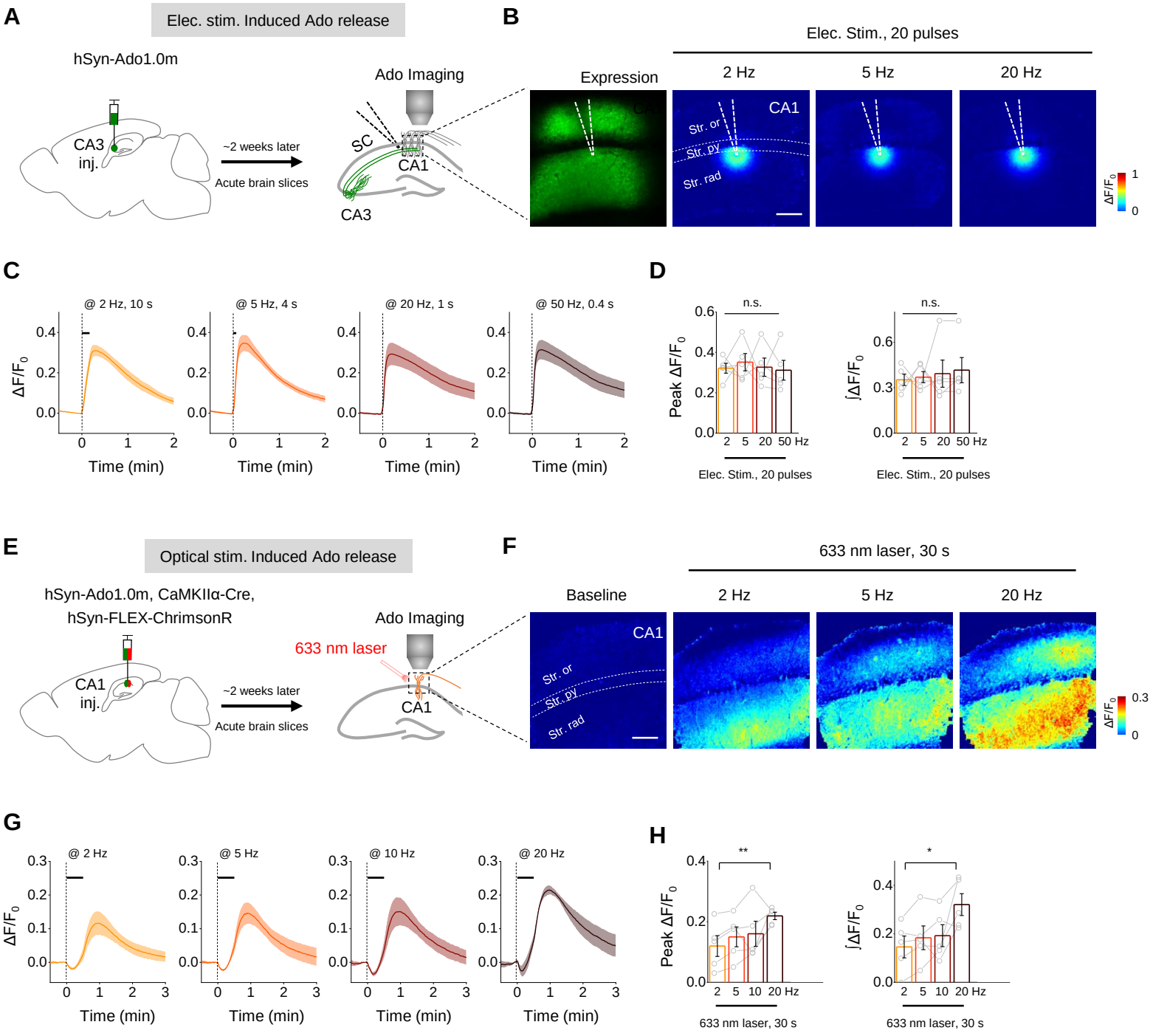

Fig. S2. Imaging local electrical stimuli and 633-nm laser stimuli induced Ado release in CA1, related to Fig. 1.

(A) Schematic illustration depicting the strategy used to image acute hippocampal brain slices prepared from mice expressing Ado1.0m in the CA3 region while using an electrode to induce Ado release in the CA1 region.

(B-D) A fluorescence image of the CA1 region showing the expression of Ado1.0m **(B, left)**. Pseudocolor images **(B, right panels)**, traces **(C)**, and group summary **(D)** of Ado1.0m $\Delta F/F_0$ in response to local electrical stimuli with the same number of stimuli (20 pulses) applied at indicated frequencies in the presence of NBQX & AP5; n = 5 slices from 2 mice.

(E) Schematic illustration depicting the strategy used to image acute hippocampal brain slices prepared from mice expressing Ado1.0m and ChrimsonR-mCherry in the CA1 region while using a 633-nm laser to activate the neurons.

(F-H) Pseudocolor images **(F)**, traces **(G)**, and group summary **(H)** of Ado1.0m $\Delta F/F_0$ in response to 633-nm laser stimuli with the same time duration (30 s) at indicated frequencies; n = 5 slices from 2 mice.

Scale bars represent 100 μm. Summary data are presented as the mean ± SEM. The data in **(D)** were analyzed using a one-way ANOVA followed by Bonferroni's Multiple Comparison Test; the difference between the 2 Hz and 20 Hz induced response in **(H)** was analyzed using Student's t-test; **p<0.01; *p<0.05; n.s., not significant.

SI Appendix Fig. S3

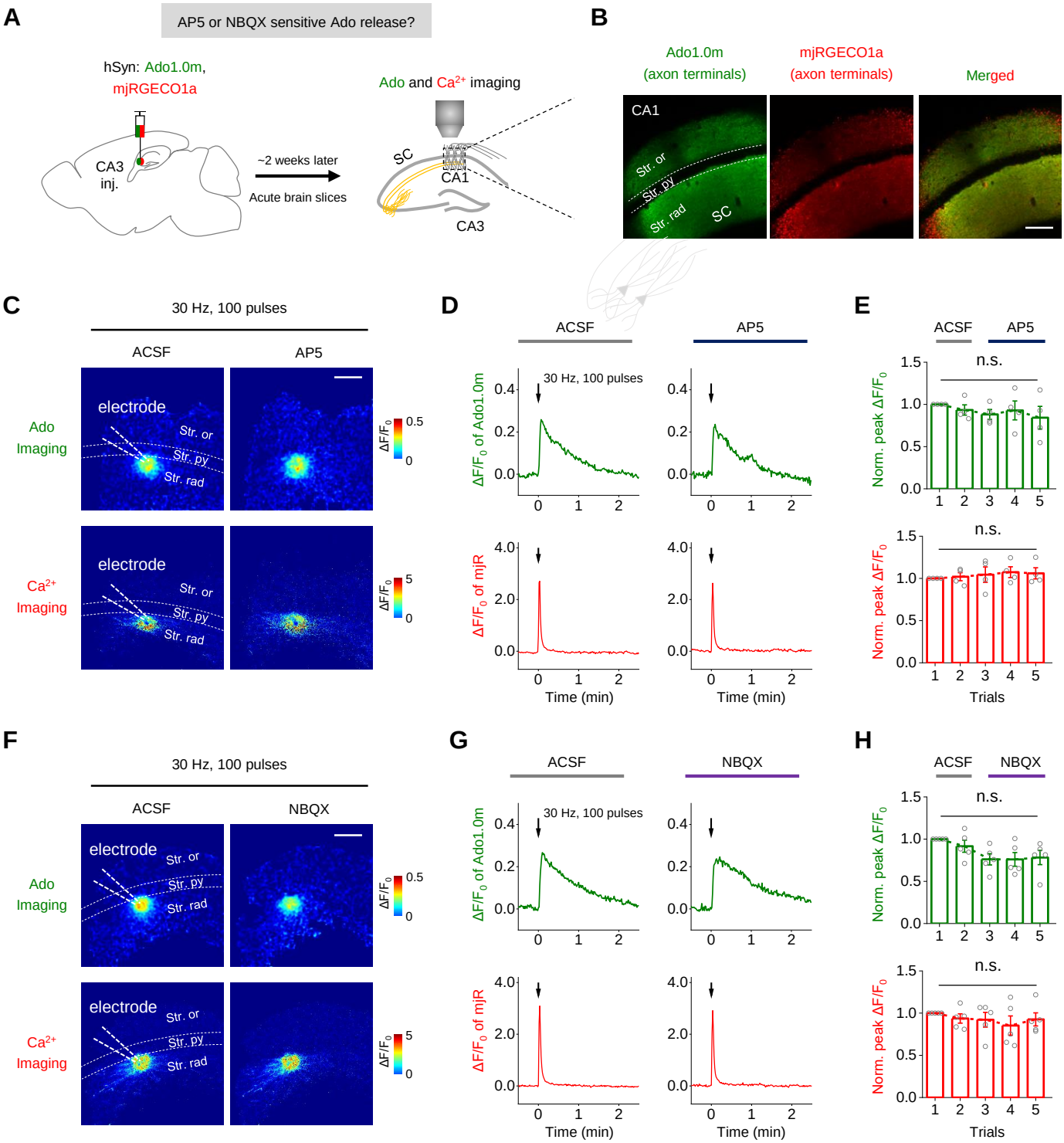

Fig. S3. The effects of NBQX alone and AP5 alone on the Ado1.0m and mjRGECO1a, related to Fig. 1.

(A) Schematic illustration depicting the strategy used to image acute hippocampal brain slices prepared from mice expressing Ado1.0m and membrane-targeted jRGECO1a (mjRGECO1a) in the CA3 region while using an electrode to induce Ado release in the CA1 region.

(B) Fluorescence images of the CA1 region showing Ado1.0m (green) and mjRGECO1a (red) in CA1 regions.

(C-E) Pseudocolor images **(C)**, traces **(D)**, and group summary (E) of Ado1.0m $\Delta F/F_0$ in response to 100 pulses applied at 30 Hz in the absence (ACSF) and presence of D-AP5; n = 5 slices from 3 mice.

(F-H) Pseudocolor images **(F)**, traces **(G)**, and group summary **(H)** of Ado1.0m $\Delta F/F_0$ in response to 100 pulses applied at 30 Hz in the absence (ACSF) and presence of NBQX; n = 4 slices from 3 mice.

Scale bars represent 50 μm. Summary data are presented as the mean ± SEM. Statistical significances in **(E and H)** were assessed using a one-way ANOVA followed by Bonferroni's Multiple Comparison Test; n.s., not significant.

SI Appendix Fig. S4

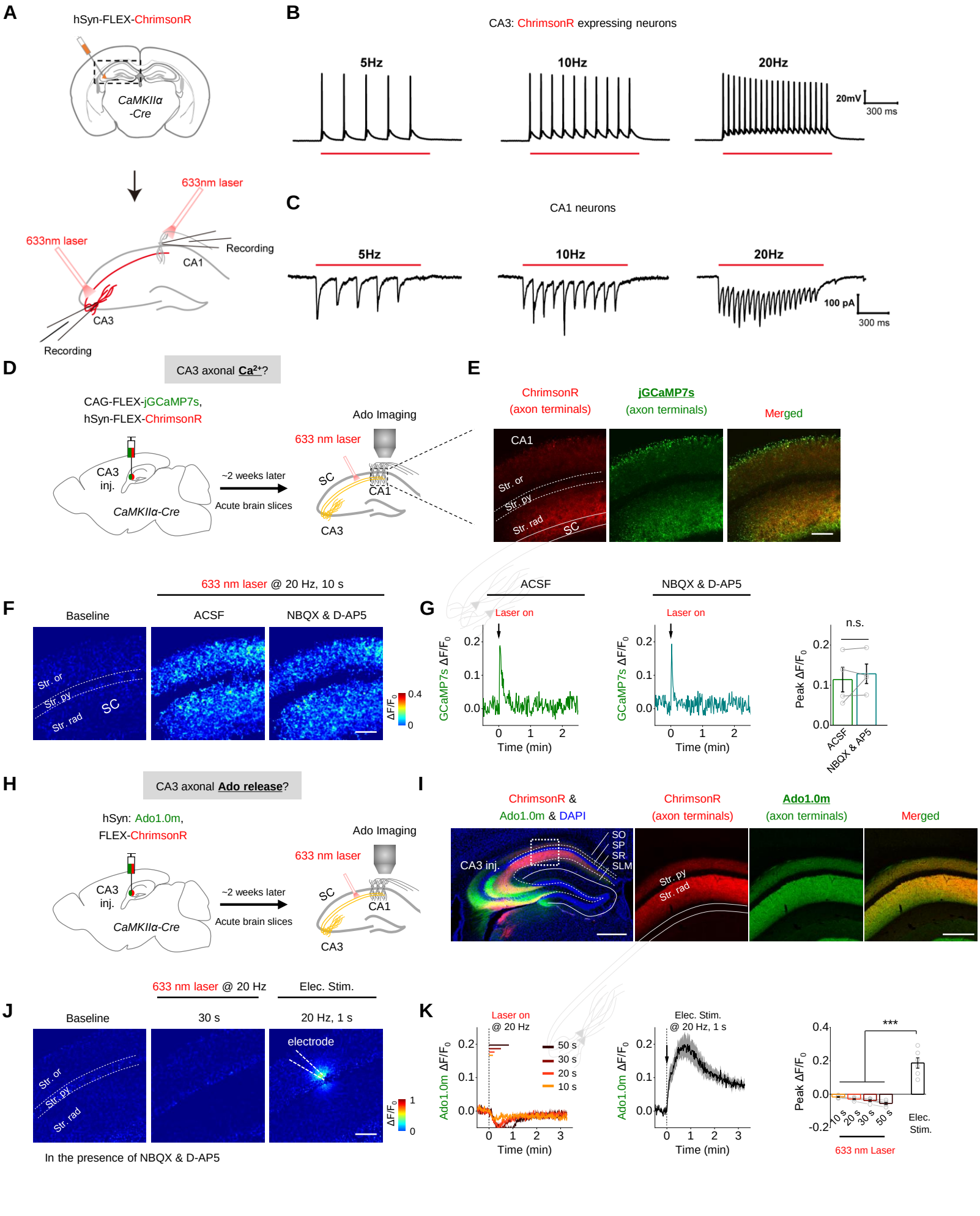

Fig. S4. Optogenetic activation of CA1 axons, related to Fig. 2.

(A) Schematic illustration depicting the strategy used to activate CA3 axon terminals in acute hippocampal brain slices prepared from mice expressing ChrimsonR in the CA3 region while using 633-nm light to activate the CA3 regions or CA3 axonal terminals in the CA1 region.

(B) Electrophysiological recordings at ChrimsonR-expressing CA3 neurons while using a 633-nm laser to activate the CA3 region.

(C) Electrophysiological recordings at CA1 neurons while using a 633-nm laser to activate the CA3 axon terminals.

(D) Schematic illustration depicting the strategy used to image acute hippocampal brain slices prepared from mice expressing jGCaMP7s and ChrimsonR-mCherry in the CA3 region while using a 633-nm laser to activate the axonal terminals in the CA1 region.

(E) Fluorescence images of the CA1 region showing jGCaMP7s (green) and ChrimsonR-mCherry (red) in CA1 regions.

(F and G) Pseudocolor images **(F)** and traces **(G)** of jGCaMP7s $\Delta F/F_0$ in response to 633-nm laser pulses applied at 20 Hz for the indicated duration; n = 4 slices from 2 mice.

(H) Schematic illustration depicting the strategy used to image acute hippocampal brain slices prepared from mice expressing Ado1.0m and ChrimsonR-mCherry in the CA3 region while using a 633-nm laser to activate the axonal terminals (Schaffer Collaterals, SC) in the CA1 region.

(I) Left, Fluorescence images of hippocampus showing the expression of Ado1.0m (green) and ChrimsonR (red). Right, magnified images of the CA1 region showing ChrimsonR-mCherry and Ado1.0m in CA1 regions.

(J and K) Pseudocolor images **(J)**, traces, and group summary **(K)** of Ado1.0m $\Delta F/F_0$ in response to 633-nm laser pulses or local electrical stimuli applied at 20 Hz for the indicated duration within the 10 μM NBQX and 50 μM D-AP5; the solid line is shown in the right panel a linear fit to the data; n = 6 slices from 3 mice.

Scale bars represent 500 μm **(I, left)** and 100 μm **(E, F and J; I, right)**. Summary data are presented as the mean ± SEM. Statistical significance in **(G)** was assessed using Student's t-test; statistical significance in **(K)** was assessed and analyzed using a one-way ANOVA followed by Bonferroni's Multiple Comparison Test; n.s., not significant; ***p<0.001.

SI Appendix Fig. S5

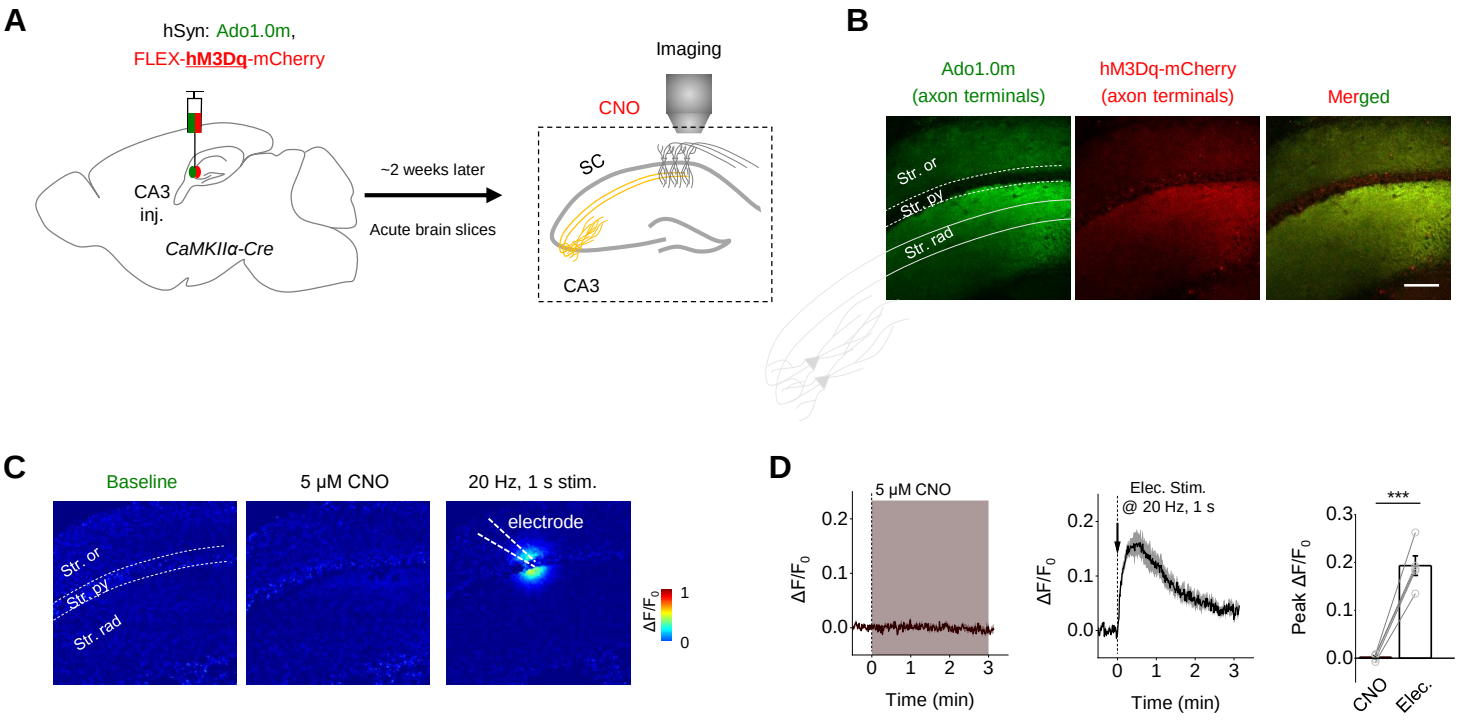

Fig. S5. No detectable chemogenetic activation-induced Ado release in CA3 axons, related to Fig. 2.

(A) Schematic illustration depicting the strategy used to image acute hippocampal brain slices prepared from mice expressing Ado1.0m and hM3Dq-mCherry in the CA3 region.

(B) Fluorescence images of the CA1 region showing Ado1.0m (green) and hM3Dq-mCherry (red) in CA1 regions.

(C and D) Pseudocolor images **(C)**, traces, and group summary **(D)** of Ado1.0m $\Delta F/F_0$ in response to 5 μM CNO application or local electrical stimuli (scale bar, 100 μm) within the NBQX (10 μM) and D-AP5 (50 μM); n = 5 slices from 2 mice.

Scale bars represent 100 μm. Summary data are presented as the mean ± SEM. Statistical significance in **(D)** was assessed using Student's t-test; ***p ≤ 0.001.

SI Appendix Fig. S6

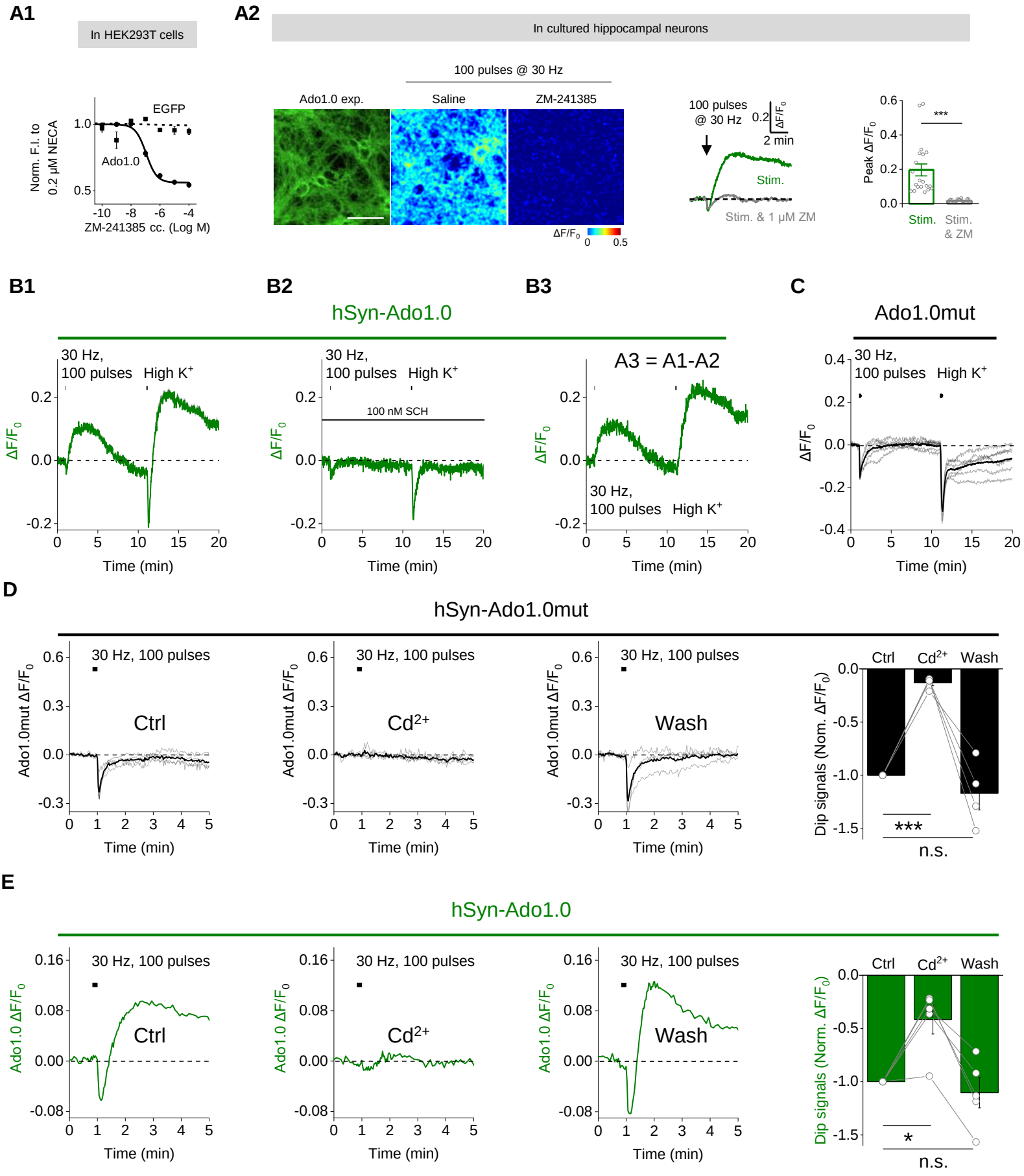

Fig. S6. Specificity of stimulation-induced Ado1.0 $\Delta F/F_0$ in cultured hippocampal neurons, related to Fig. 3.

(A1) Dose-dependent curves for Ado1.0 sensor or EGFP-CAAX control in HEK293T cells in response to ZM-241385. To induce Ado1.0 response, 0.2 μM NECA, an $A_{2A}R$ agonist, was used.

(A2) Traces, peak $\Delta F/F_0$, and summary for Ado1.0 sensor in cultured hippocampal neurons in response to 100 pulses applied at 30 Hz in the absence (ACSF) and presence of ZM-241385 (1 μM); n = 20 ROIs /5 coverslips.

(B) Exemplar traces of $\Delta F/F_0$ measured in Ado1.0-expressing cultured hippocampal neurons in response to 100 field stimuli delivered at 30 Hz and high K^+ in the absence **(B1)** and presence **(B2)** of SCH-58261 (SCH, 100 nM). **(B3)** shows the subtracted trace.

(C) Traces showing Ado1.0mut $\Delta F/F_0$ in response to 100 field stimuli at 30 Hz and high K^+ (n = 6 coverslips).

(D and E) Ado1.0mut **(D)** and Ado1.0 **(E)** $\Delta F/F_0$ were measured in response to 100 field stimuli delivered at 30 Hz before (Ctrl), during, and after (Wash) application of Cd^{2+} (200 μM). Summary data are shown at the right, normalized to control; n = 4-5 coverslips per group.

The scale bar represents 100 μm. Summary data are presented as the mean ± SEM. Statistical significance was assessed by Student's t-test. n.s. not significant, *$p \leq 0.05$, ***$p \leq 0.001$.

SI Appendix Fig. S7

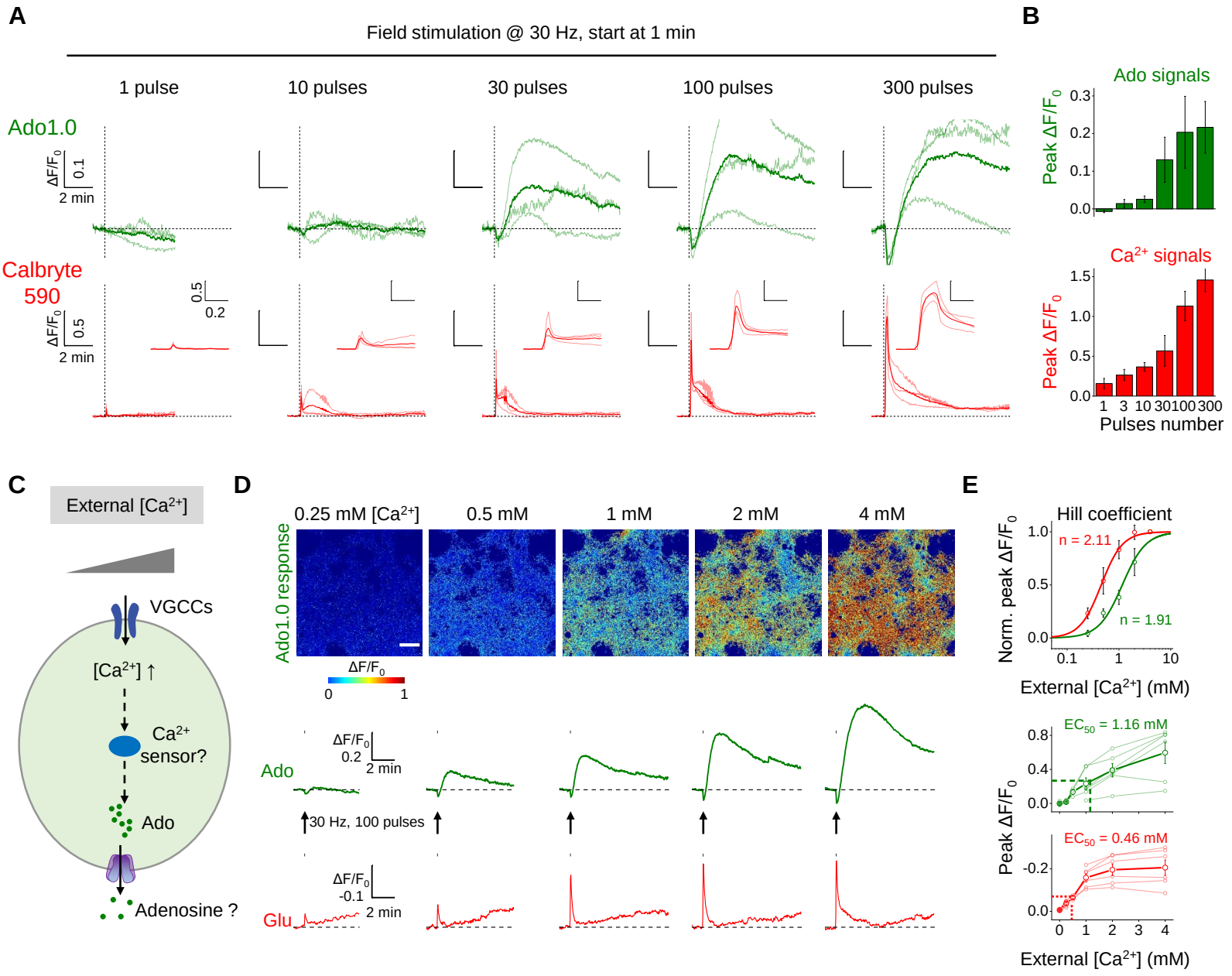

Fig. S7. Simultaneously detecting Ado and Ca^{2+} signals or Ado and glutamate signals, related to Fig. 3 and Fig. 5.

(A and B) Two-color imaging of Ado and Ca^{2+} signals from the same neurons. Traces **(A)** and group summary **(B)** of Ado1.0 and the Ca^{2+} indicator Calbryte 590 $\Delta F/F_0$ in response to the indicated number of field stimuli applied at 30 Hz. In **(A)**, the thin lines represent individual cells, and the thick lines represent the average trace; insets in the lower row meant a magnified view of 0.8-1.5 min of traces; n = 3 coverslips.

(C-E) Ca^{2+} sensitivity differs between Ado release and Glu release. **(C)** Schematic drawing depicting the experimental strategy. Dual-color imaging was used to image Ado and Glu release in various concentrations of extracellular Ca^{2+}. **(D)** Pseudocolor images (top) and traces (bottom) of Ado1.0 and R^{ncp}-iGlu $\Delta F/F_0$ in response to field stimuli (30 Hz, 100 pulses) in the indicated concentrations of extracellular Ca^{2+}. **(E)** Summary of peak Ado1.0 and R^{ncp}-iGlu $\Delta F/F_0$ (n = 6 coverslips); the data in the top panel were normalized to the peak response measured in 4 mM Ca^{2+}, and the data were fitted with a Hill equation (see main text).

Scale bars represent 100 μm. Summary data are presented as the mean ± SEM.

SI Appendix Fig. S8

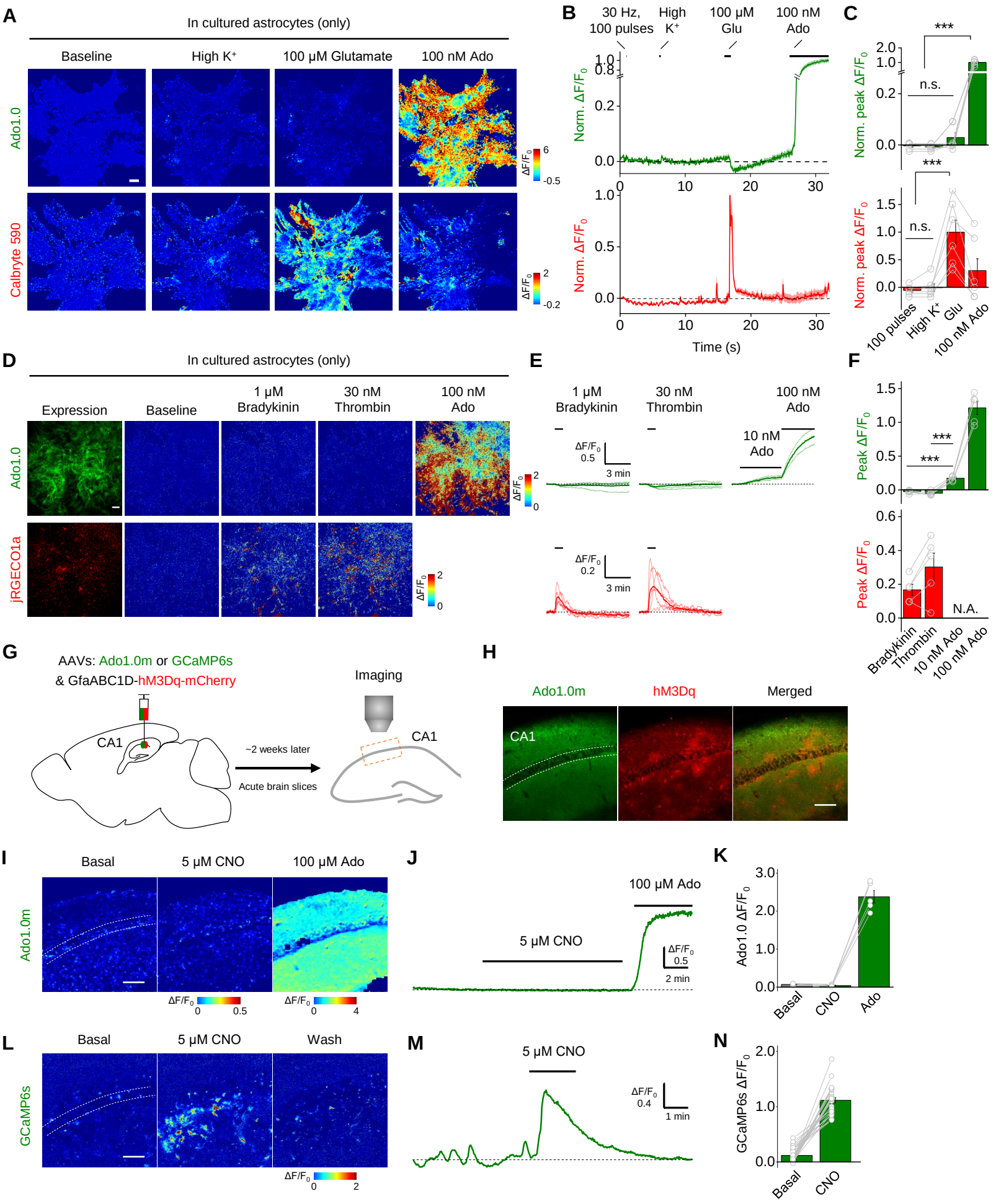

Fig. S8. Not detectable Ado release from astrocytes in cultures and acute brain slices, related to Fig. 3. and Fig. 6.

(A-C) Dual-color imaging of Ado1.0 (upper panels) and Calbryte 590 (Cal 590, bottom panels) in response to 100 field stimuli at 30 Hz, high K^+ (75 mM KCl), 100 μM glutamate (Glu), or 100 nM Ado, in cultured astrocytes. Exemplar pseudocolor images **(A)**, exemplar traces **(B)**, and summary data **(C)** are shown; n = 6 coverslips each.

(D-F) Dual-color imaging of Ado1.0 (upper panels) and NES-jRGECO1a (bottom panels) in response to 1 μM bradykinin, 30 nM thrombin, 10 nM Ado or 100 nM Ado, in cultured astrocytes.; confocal or pseudocolor images **(D)**, traces **(E)**, and group summary **(F)** are shown; n = 5 coverslips. N.A., not available.

(G-N) Imaging of Ado1.0m and GCaMP6s responses in acute brain slices. To activate astrocytes, hM3Dq-mCherry was expressed driven by a GfaABC1D promoter; clozapine N-oxide (CNO, 5 μM) was used; to image extracellular Ado, Ado1.0m was expressed driven by a hSyn promoter; to image astrocytic Ca^{2+}, GCaMP6s was expressed driven by GfaABC1D promoter; n = 5 brain slices from 2 mice for Ado1.0m group; n = 29 astrocytes from 2 mice for GCaMP6s group.

Scale bars: 100 μm. Summary data are presented as the mean ± SEM. The data in **(C)** and **(F)** were analyzed using Student's t-test; ***p<0.001; n.s., not significant.

SI Appendix Fig. S9

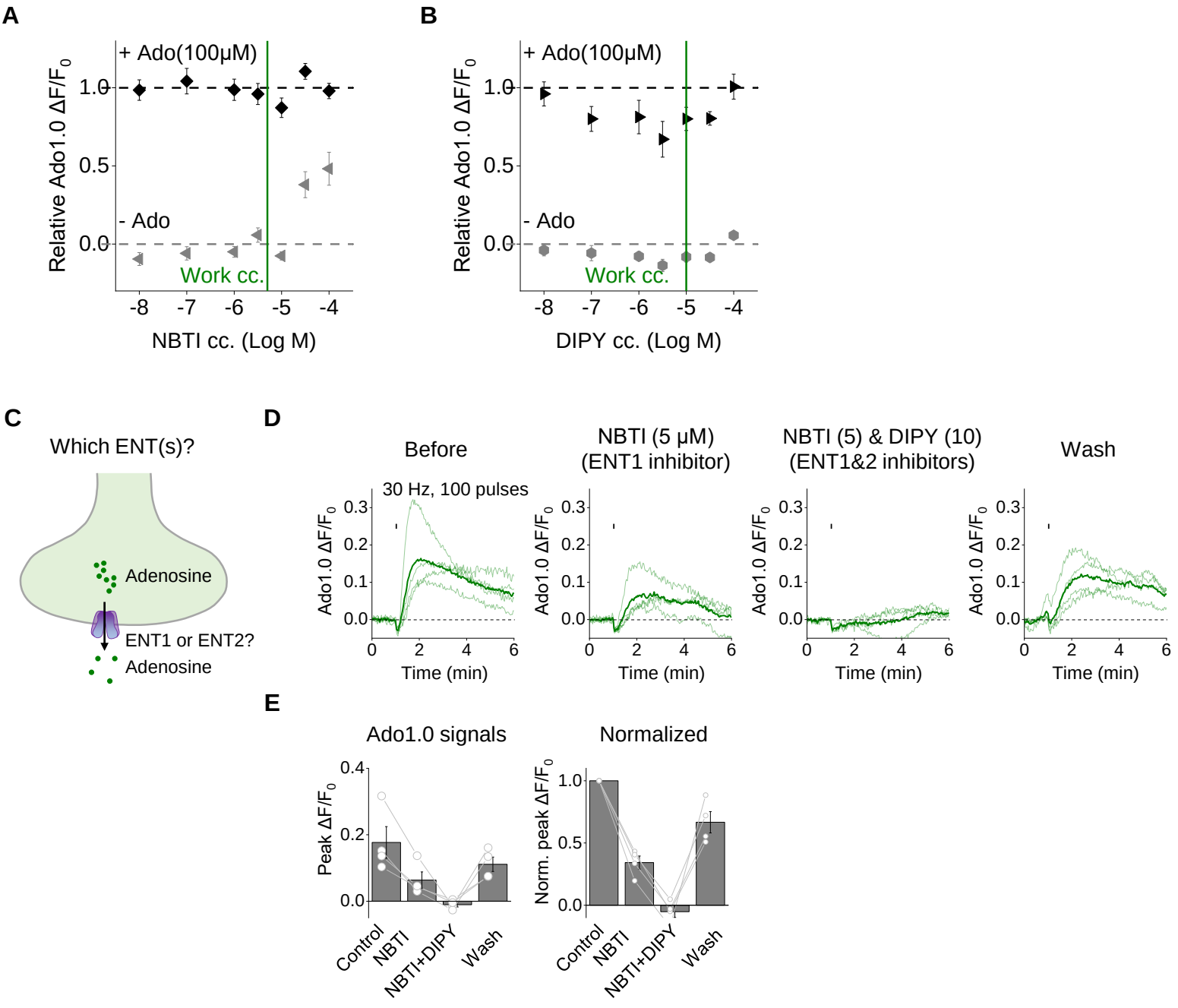

Fig. S9. Both ENT1 and ENT2 contribute to the activity-dependent Ado release, related to Fig. 4.

(A and B) S-(4-nitrobenzyl)-6-thioinosine (NBTI) and dipyridamole (DIPY) did not affect the responses of Ado1.0 at the concentrations of use.

(C) Schematic drawing depicting the putative mechanism by which equilibrative nucleoside transporters (ENTs) mediate Ado release in neurons.

(D and E) Traces **(D)** and group summary **(E)** of Ado1.0 $\Delta F/F_0$ in response to field stimuli (30 Hz, 100 pulses, indicated by black tick marks) before (control), during, and after (wash) application of the ENT1 blocker NBTI (5 μM) and/or the ENT1/2 blocker dipyridamole (DIPY, 10 μM); n = 4 coverslips.

Summary data are presented as the mean ± SEM.

SI Appendix Fig. S10

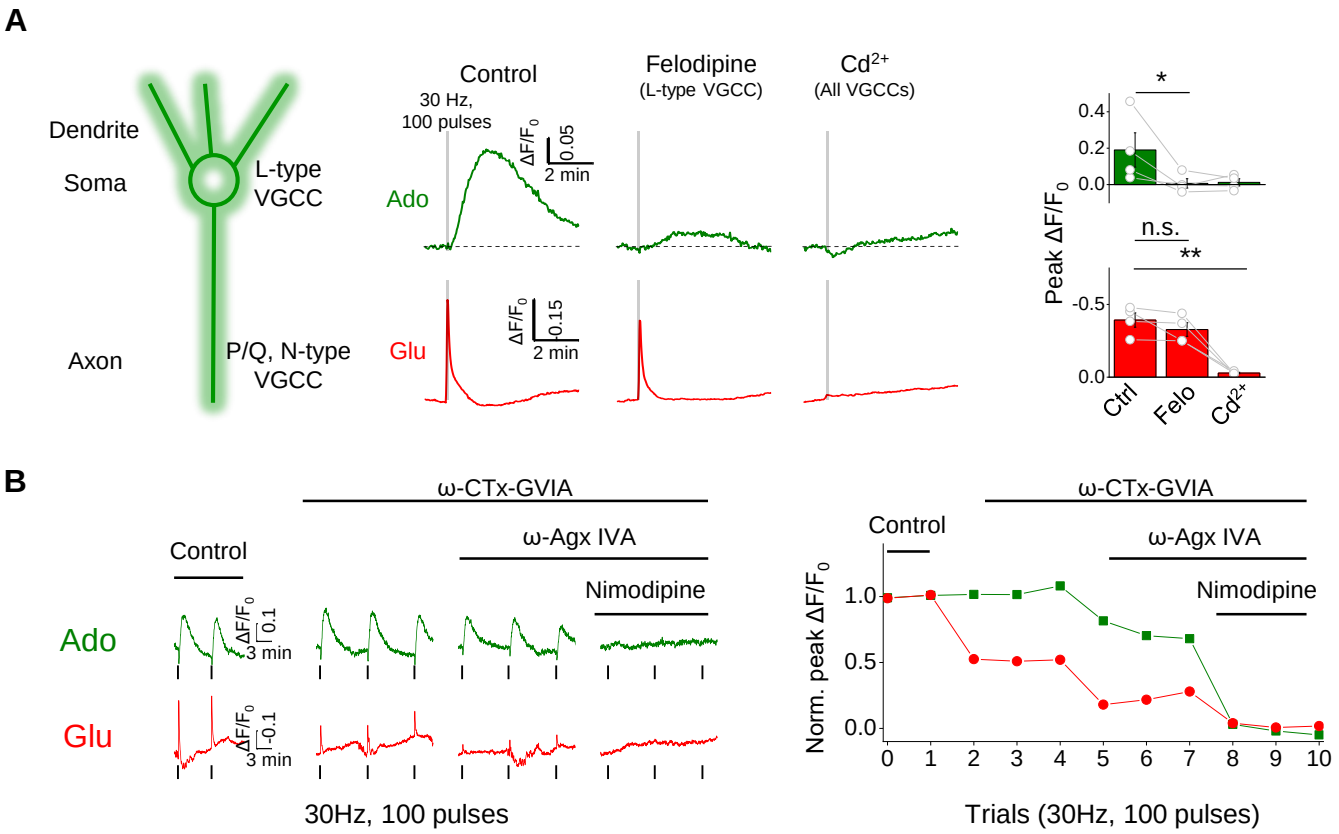

Fig. S10. Calcium sources of activity-dependent Ado release, related to Fig. 5.

(A) Blocking L-type voltage-gated calcium channels (VGCCs) inhibit Ado release. Left panel: cartoon illustrating that L-type VGCCs are expressed primarily in the somatodendritic compartment, while P/Q-type and N-type VGCCs are expressed primarily in the axon. Middle panels: example traces of Ado1.0 and R^{ncp}-iGlu $\Delta F/F_0$ in response to field stimuli (30 Hz, 100 pulses) delivered before (control), during, and after (wash) application of either the L-type VGCC blocker felodipine (Felo, 10 μM) or Cd^{2+} (200 μM). Right: group summary of Ado1.0 (top panel) and R^{ncp}-iGlu (bottom panel) $\Delta F/F_0$ in response to field stimuli; n = 4 coverslips each. The data in the control group are the same as in Fig. 4D.

(B) Example traces and normalized peak Ado1.0 and R^{ncp}-iGlu $\Delta F/F_0$ in response to field stimuli (30 Hz, 100 pulses) applied in the presence of ω-CTx-GVIA (1 μM), ω-Agx-IVA (0.3 μM), and nimodipine (10 μM) to block N-type, P/Q-type, and L-type VGCCs, respectively (the same coverslip was sequentially treated with the indicated blockers).

(C) Confocal images of cultured hippocampal neurons co-expressing Ado1.0 (green) and mCherry-tagged CaMKIIα-hM3Dq (red).

The scale bar represents 100 μm. Summary data are presented as the mean ± SEM. Statistical significance was assessed by a two-tailed Student's t-test. n.s. not significant, *p ≤ 0.05, **p ≤ 0.01.

SI Appendix Fig. S11

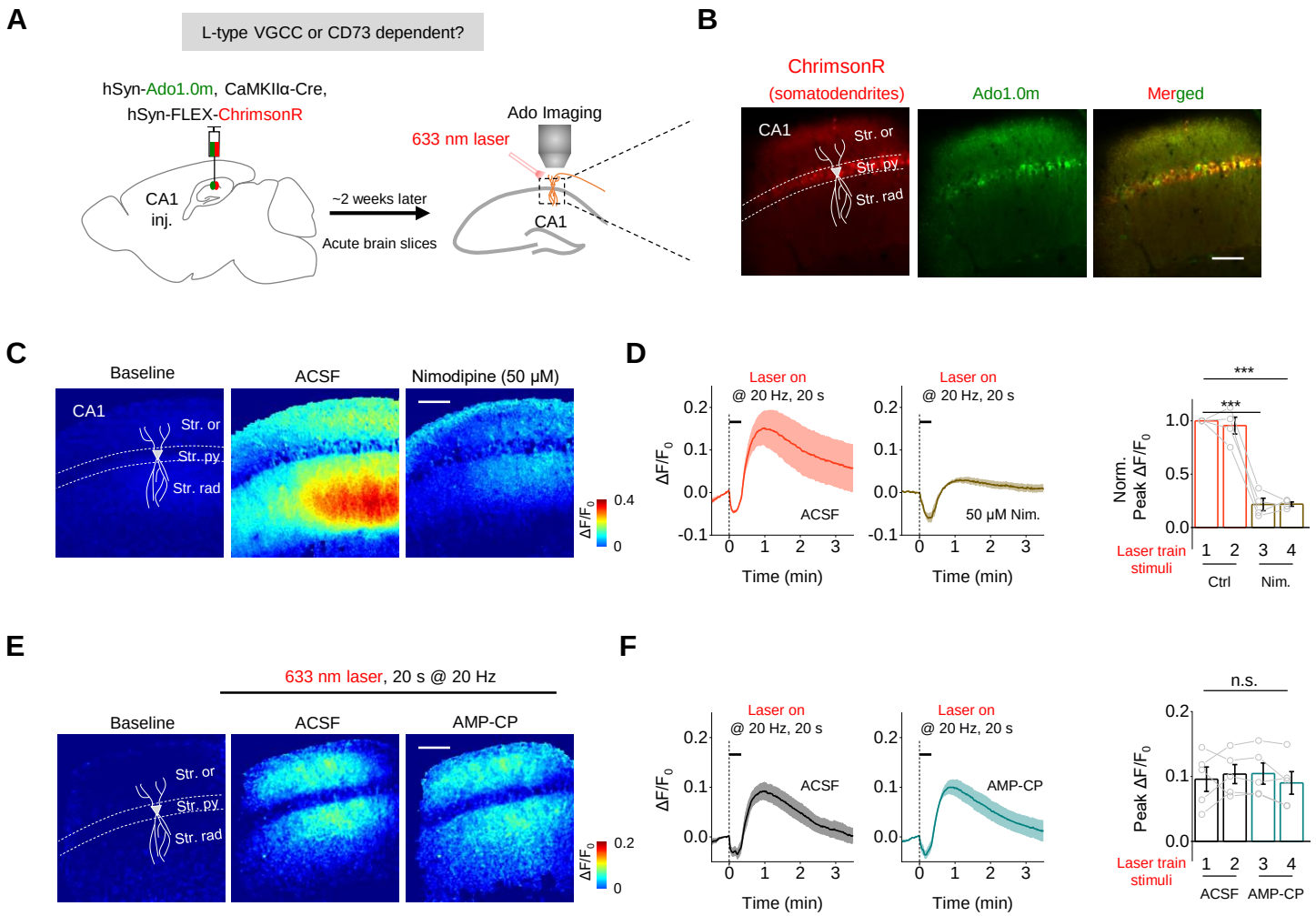

Fig. S11. L-type VGCC dependent and CD73 independent Ado release in hippocampal brain slices, related to Fig. 6.

(A) Schematic illustration depicting the strategy used to image acute hippocampal brain slices prepared from mice expressing Ado1.0m and ChrimsonR in the CA1 region while using a 633-nm laser to activate the CA1 region.

(B) Florescence images showing ChrimsonR-mCherry (red) and Ado1.0m (green) in CA1 regions.

(C and D) Images **(C)**, traces, and group summary **(D)** of Ado1.0m $\Delta F/F_0$ in response to 633-nm laser pulses applied at 20 Hz for 20 s in the absence (Ctrl) and presence of 50 μM nimodipine (Nim); n = 4 slices from 2 mice.

(E and F) Pseudocolor images **(E)**, traces, and group summary **(F)** of Ado1.0m $\Delta F/F_0$ in response to 633-nm laser pulses applied at 20 Hz for 20 s in the absence (ACSF) and presence of a CD73 inhibitor, α,β-Methyleneadenosine 5'-diphosphate (AMP-CP, 10 μM); n = 5 slices from 2 mice.

Scale bars represent 100 μm. Summary data are presented as the mean ± SEM. Statistical significance was assessed by a one-way ANOVA followed by Bonferroni's Multiple Comparison Test; ***$p \leq 0.001$; n.s. not significant.